GENERAL GEOLOGY OF LIMESTONE IN THE F-FIELD OF CENTRAL LUCONIA WITH EMPHASIS ON PORE NETWORK MAPPING

By

Low Zoann
13860

Progress Report submitted in partial fulfillment of
the requirements for the
B. Technology of Geoscience (Hons)
(Petroleum Geoscience)

FYP II Semester and Year

February 2014

Universiti Teknologi PETRONAS
Bandar Seri Iskandar
31750 Tronoh
Perak Darul Ridzuan

CERTIFICATION OF APPROVAL

GENERAL GEOLOGY OF LIMESTONE IN THE F-FIELD OF CENTRAL LUCONIA WITH EMPHASIS ON PORE NETWORK MAPPING

by

Low Zoann

13860

A project dissertation submitted to the

Petroleum Geoscience Programme

Universiti Teknologi PETRONAS

in partial fulfilment of the requirement for the

BACHELOR OF TECHNOLOGY (Hons)

(PETROLEUM GEOSCIENCE)

Approved by,

_____

(Assoc. Prof. Dr. Eswaran Padmanabhan)

UNIVERSITI TEKNOLOGI PETRONAS

TRONOH, PERAK

September 2014

CERTIFICATION OF ORIGINALITY

This is to certify that I am responsible for the work submitted in this project, that the original work is my own except as specified in the references and acknowledgements, and that the original work contained herein have not been undertaken or done by unspecified sources or persons.

_____

LOW ZOANN

ABSTRACT

Dissolution has played a significant role in the modification of reservoir properties, specifically in the distribution of porosity and permeability within the carbonate bodies which directly affect reservoir performance. For rigorous reservoir characterization and performance prediction from petrophysical measurement, interpretation of the micropores behavior of different carbonate pore types is crucial due to its complex pore network. In order to improve our detail understandings of the pore behavior of the carbonate buildups in Central Luconia, a thorough investigation of the pore network was undertaken in two F-field wells from the Central Luconia Basin of Sarawak, Malaysia. The goal of this study was to testify the pore behavior of the carbonate rocks under several acid treatments by quantifying the changes of its pore geometry and spatial distribution of the rocks. Additional onshore carbonate analogue mapping in Sungai Siput, Perak was done prior to understand the offshore carbonate buildups. Core analysis to identify the offshore samples facies from drilled cores was done coherently with fabric classification using standard carbonate quantification manual. Initial pore network imaging and quantification of selective facies was then scrutinized through several petrographical analyses i.e. x-ray diffraction (XRD), thermal conductivity, energy dispersive x-raty (EDX), petrography, Poroperm, scanning electron microscopic analysis (SEM) and CT scan. Examination of post dissolution pore network like atomic absorption spectrometry (AAS) and CT-Scan were carried out after dissolution kinectics test was introduced. Results showed that carbonate rocks subjected to acid treatment on a prolong period of time exhibit prominent increment and enlargement in terms of pore geometry and spatial distribution.

ACKNOWLEDGEMENT

Foremost, I would like to express my sincere gratitude to my supervisor Assoc. Prof. Dr. Eswaran Padmanabhan for the continuous support of my Final Year Project, for his patience, motivation, enthusiasm, and immense knowledge. His guidance helped me in all the time of running the research from field work to thesis writting. I could not have imagined having a better advisor and mentor for my FYP.

Besides my advisor, I would like to specially thank Mr Andriamihaja Spari and the fellow geochemistry post graduate students for their insightful comments and helping hands in explaining and guiding me with all the laboratory experiment theories and details.

Last but not the least, I would like to thank my parents who had supported me spiritually throughout my whole undergraduate studies, this has made my journey in University Technology PETRONAS the meaningful ones.

TABLE OF CONTENTS

LIST OF FIGURES

LIST OF TABLES

CHAPTER 1

INTRODUCTION

1.1 Background

Central Luconia

Carbonates buildups in the Central Luconia Province of Sarawak had long been discovered and many wells were drilled in feed of the gas demand worldwide. The Central Luconia Province is indeed a broad and stable continental shelf platform, characterized by the extensive development of Late Miocene carbonates as the highlight. The formation of the carbonates in Central Luconia can be traced back from the spreading of South China Sea during Oligocene. Subduction of South China Plate beneath Borneo created an orogenic belt contributing to the supply of nutrient-rich water to the Sarawak shelf and caused the growth of carbonate buildups from Middle to Late Miocene.

The size and distribution of the buildups in Central Luconia are structurally-controlled by the pre-development of horst-graben from crustal extension (Ali & Abolins, 1999). Large platform-type buildups developed on highs, whereas pinnacle-type buildups were formed at stronger subsidence area and closer to the source of clastic materials. Unlike the Eastern Malaysia basin, the sequential order of the stratigraphy in Sarawak is designated with ‘cycle’. Central Luconia in total has 8 regressive cycles with cycles III, IV and V carbonates as the major hydrocarbon plays, starting from the early to late Miocene.

On the other hand, Epting (1980, 1989) suggests that there are four major processes that define the buildups here in Central Luconia, (a) rate of skeletal carbonate production, (b) driving subsidence, (c) sea-level fluctuation, (d) supply of clastic materials from deltas. In theory, the quality of the Central Luconia carbonate reservoir also depends on the development and preservation of the primary porosity that is very much affected by the diagenesis processes like cementation with meteoric aquifers, burial leaching and the fluid pathways.

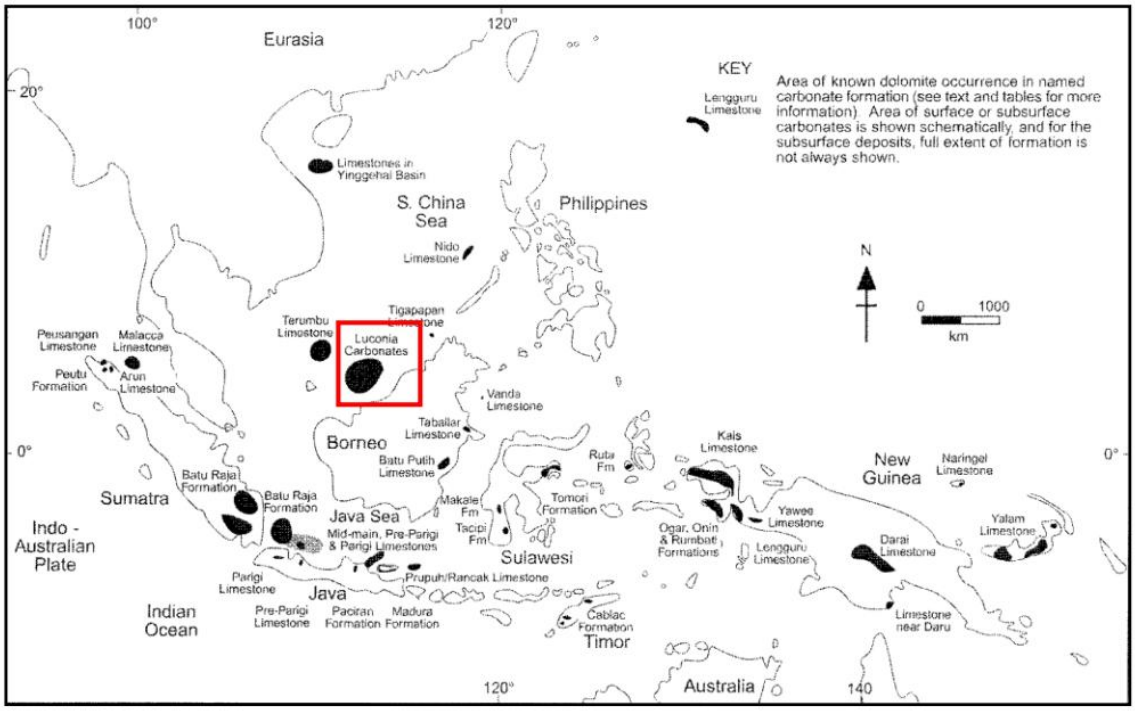

Figure 1.1: Central Luconia province (red-box).

In fact, the Central Luconia Province is one of the major hydrocarbon producing areas in the Sarawak Basin, in East Malaysia. It is also one of the largest carbonate provinces in Southeast Asia, covering an area of 240 km by 240 km. Over 200 carbonate build-ups, ranging in size from a few km^2 to more than 200 km^2 have been seismically mapped in Central Luconia. About 65 carbonate build-ups have been tested and to date, 56 of them are proven to contain commercial quantities of non- associated gas (Ali & Abolins, 1999; Epting, 1980). With a total of 40 TSCF of gas initially in place and over 30 TSCF of ultimately recoverable gas, the Central Luconia Province contains about 40%

of the total non-associated gas reserves of Malaysia (Ali & Abolins, 1999). Figure 1.1 has shown that Central Luconia is potentially accommodating the most reserves in area as compared to other carbonate reservoir in South East Asia, suggesting that future focus and research should lay on enhance oil recovery (EOR) in order to maximize the resources it opt to provide.

In this paper, diagenesis or in particular dissolution diagenesis, is the main focus of the studies of detail pore network in carbonate rocks. It is one of the major contributors to the changes of petrophysical properties of the rocks and has significant impact on reservoir quality of carbonates. Surface and shallow diagenesis mainly occurs in fabric-selective pore geometries that allow the greatest fluid flow (mostly interparticle or intercrystalline). Late-stage shallow diagenesis mainly occurs in nonfabric-selective pore geometries that allow the greatest fluid flow (mostly fracture related). Deep diagenetic processes can be both fabric selective (fluid flow through interparticle or intercrystalline pores) or nonfabric selective (compaction).

The impact of the different carbonate facies on pore network and subsequent development under various treatments however, are still not well understood. Therefore, the main objective of this study is to further investigate the impact of dissolution on pore network in the limestone of Central Luconia basin by understanding its rock fabrics in relation to the depositional environment of the limestone buildups. In fact, pore-network models have been used to describe a wide range of rock properties from porosity, pore distribution, permeability and etc. this is then further contributing to future Enhanced Oil Recovery (EOR) development and also reservoir modeling.

Sungai Siput

This research is proposed to map an analogue limestone hills near Sungai Siput, Perak in order to construct a 3-dimensional model of carbonate formation that could be used as a standard comparative model to the offshore carbonate platforms. Detail stratigraphic logging of the onshore outcrop, with additional sedimentary and post-sedimentary features observations and fabric analyses would provide information about

the temporal and lateral distribution in all scales from micrometer to meters. The goal is to produce a general view of onshore limestone depositional environment and post diagenetic events in hope to gain enlightenment for and link similarity with the offshore samples.

Geologically Sungai Siput is the most northern part of the famous Kinta Valley, stretching all the way down south from Kampar, Perak. The formation of limestone hills in Sungai Siput is associated with the Kinta Valley limestone and sharing similar geological features. In general, the valley floor of Kinta is made up of Old Alluvium or the Simpang Formation overlain bounger Alluvium or the Beruas Formation (Raj et al 2009). Older metamorphic rocks are exposed as the bedrock within this valley or stood up as isolated hills above the valley floor, while intrusive rocks form mountains on both eastern and western slopes of the basin. The geology of Kinta Valley and its surrounding area was well-described and illustrated by Ingham & Bradford (1960). It started during the Silurian time with the deposition of the clastic sediment in a relatively deep marine setting followed by the deposition of limestone following the progressive shallowing of the sea floor. This is evidence by the presence of rich shallow marine benthic organisms within the Kinta Limestone from Devonian to Permian age. Both of these clastic and calcareous Palaeozoic rock formations were intruded by acidic igneous rocks during the Late Triassic-Early Jurassic time. This intrusion formed the Main Range, Kledang Range and Bujang Melaka Granites which comprised mainly of coarse grained porphyritic biotite granites. These are S-type granites formed due to the collision between the Sibumasu and the East Malaya Block. This intrusion was also responsible in transforming the older sedimentary rocks into marble and schist and the deposition of rich tin and iron ores during its late phase emplacement.

Following the collision of Sibumasu-East Malaya, Peninsular Malaysia was uplifted to form a new terrestrial environment and to allow exogenic processes to take place. The Post Triassic exogenic geological processes have eroded weaker rocks and formed the Kinta Valley prior to the deposition of the Simpang Formation and rich plaser tin deposits and have etched the limestone to form several cock-pit and isolated tower karst with many small and large cave.

In terms of litholgy, Kinta Valley's limestone is made largely of calcite or calcium carbonate or dolomite. It is mostly white, pale grey or tinged with yellow although there are variations due to the presence of iron. Marble is found in some hills. Erosion at the base of the outcrops has resulted in the formation of caves. The caves are magnificent both in size, features and in some instances, biological life. The limestone hills and caves are located between Kanthan, in the north and Kuala Dipang, in the south (Ipoh Echo, 2012). Stratigraphic record of Sungai Siput shows that the limestone hills there are mainly dominated by thinly laminated mudstone to wackestone with occasional breccia blocks. They are part of the Kinta Valley limestones which are relicts of thick Paleozoic carbonate deposits, mainly Carboniferous to Permian in age. Slumping is common throughout the section, and is enhanced by beds of chert which are initially interbedded with micritic limestone. A preliminary interpretation indicates that the slump structures were formed with plastic-ductile deformation on a slope within deep marine environment. The slope is dipping to the west with an approximately N-S strike direction, suggesting the presence of a platform paleomargin, probably with grainy deposits (Kadir, Pierson, Harith, & Chow, 2009).

Limestone are likely similar in terms of characteristics albeit differences in some properties like post-sedimentary features and facies. Thus, the Sungai Siput limestone can be served as a suitable analogue modal to the Central Luconia carbonate buildups, in hope of making detail relation even to micrometer in scales.

1.2 Problem Statement

The textural, physical and chemical properties of limestones are often controlled by diagenetic reactions involving dissolution of carbonate minerals. The post sedimentary alteration of carbonate rocks after dissolution has designated variation of carbonate characteristics in terms of petrophysical properties. Albeit many studies has focused on characterizing the carbonate pore network, the impact of dissolution on different carbonate facies pore network, however, is still not well understood, especially at the F-

fields of Central Luconia carbonate platform. There still exists a gap of knowledge about the pore behavior of the carbonate after diagenesis.

On the other hand, carbonate facies heterogeneity not only exists within the same well, it also varies at different location on the carbonate platform. The formation Central Luconia buildups needed more investigation on depositional environment as well as temporal facies distribution across the platform. This is to be achieved by mapping analogue onshore carbonate outcrop of Sungai Siput, that in hope be used as a comparative model to compare and contrast with the offshore platform and impart knowledge about the carbonate depositional environment.

1.3 Objectives

1. To study the similarities and resemblance of the onshore outcrops with the offshore samples.
2. To evaluate the sedimentology and general geology in Central Luconia.
3. To evaluate the difference in fabric and spatial distribution of the selective core facies.
4. To evaluate the changes of the pore network within the selective core facies after dissolution kinetics.

1.4 Scope of study

The main focus of this paper is to understand the sedimentology and general geology of the Central Luconia province both theoretically and physically. First, the geological studies on Central Luconia is understood based on the reviewed literature of depositional environment and the regional tectonic history affecting or contributing to the carbonates buildups in Sarawak. Second, an analogue mapping of Sungai Siput onshore outcrops is performed to answer some geological research questions about carbonate rocks and link the resemblance of which to the offshore samples.

In terms of sampling, this paper focused mainly on the carbonate core samples of Central Luconia rocks that were collected from core warehouse of PETRONAS Geo Sample Center located in Ampang, Selangor. Both F41 field and F61 field cores were

cored at the year of 80s and then stored in the warehouse. The condition of the core samples was seemingly fair and 30% of it had been cut off to run other field tests during the period of 30years. Understanding of the cut off is done by estimating or upscalling from the remaining cores. The F61 well was cored at the depth of 3706ft to 3757ft at the estimated age of Middle Miocene, coring through the studying lithology – carbonate buildups. Similarly to F41 well, core was at the depth of 1238ft to 1243ft also coring through the carbonate buildups.

Chemical and physical tests to examine the pore network changes is focused from plug sized core scale to microscopic scale, in order to observe the changes in details. The significance of performing lab tests on the samples is to build a bridge between the gaps of knowledge about the pore behavior and also to predict the connectivity of the pores after dissolution treatment. This might then be useful in future Enhanced Oil Recovery simulation and also better improvised model for reservoir characterization and modeling after production at some times.

In its entirety, the understanding of the offshore carbonate buildups in Central Luconia were mainly done by seismic and also well tie integration techniques where the subsurface carbonate platforms still lacking of reality. Although core studies might narrow the gap of knowledge about the subsurface, heterogeneity still a major tripping stone on stereotyping the subsurface condition solely based on the tenth meter scaled core that only confirms the vertical distribution. Therefore, it is ordered to quantity the spatial distribution the F41 and F61 wells for better understanding of the pore behavior in the complex pore network of carbonates.

CHAPTER 2

LITERATURE REVIEW

Carbonates can exhibit highly varying properties (e.g., porosity, permeability, flow mechanisms) within small sections of the reservoir, making the study of carbonates reservoir rocks rather tricky due to its heterogeneity in terms of spatial distribution and petrophysical properties. A focused approach is needed to better understand the heterogeneous nature of the rock containing the fluids and the flow properties within the porous and often fractured formations. This involves detailed understanding of the fluids saturation, pore-size distribution, permeability, rock texture, reservoir rock type, and natural fracture systems at different scales.

As the nature of carbonates goes, the porosity and permeability of a carbonate reservoir are majorly controlled by:

- Effect of digenesis that evolves through geological history, e.g. cementation, recrystalization, dissolution and etc.
- Environmental condition that determines the carbonates growth, e.g. energy, light, temperature, climate, water depth and etc.
- Primary depositional environment that contributes to the primary spatial distribution and hence the primary porosity.

Since carbonates are sensitive to their surrounding environment, understanding both the current geological environment and palaeoenvironment of the place of interest come forward as precedence in obtaining in-depth information. The geological settings in Central Luconia were best described by Epting (1980) and Ali and Abolins (1999) however, the seismic illustration about the carbonates buildups in Central Luconia was

actually published by Hutchison recently. In his paper, the seismic sections had shown more than 200 carbonate buildups in the area and the large-platform with adjacent pinnacles had been dated from the Middle to Upper Miocene which then died out afterward. This is understood that, the surviving environment of the coral reefs were unfavorable that time due to the changes of eustatic sea level as well as the influx of clastic sediment massively depositing on the corals. On top of which, during the Early Miocene to Late Miocene times, offshore southeast Asia was characterized by the development of shallow-water carbonates and reefs, strongly influenced by the interplay between sea-level and basinal tectonics (King, Chung, & AlJaaidi, June 2010).

Debate rise however, how much influence does the original fabric of a carbonate rock (grains, mud, and pore space) have on with the pore space in the rock now? Which has more impact on reservoir quality of carbonates: early or late diagenesis? The interaction of early diagenesis with original fabric elements determines, in many cases, the ultimate reservoir quality of a carbonate. A rock that begins with good porosity and permeability, either from depositional or early diagenetic processes, has a better chance of retaining those qualities than an initially poor-quality rock becoming a good-quality rock. Porosity can be created late in a rock's life; however, concentrating on the early history of a carbonate rock is generally more rewarding when searching for reservoir-quality rocks. (Hartmann & Beaumont, 2000)

The flow characteristics of carbonate reservoirs are controlled by a combination of depositional and diagenetic processes. Depositional processes control the initial pore size distribution and the geometry of the individual depositional facies. The diagenetic overprint modifies the pore size distribution and controls the productivity of depositional facies. In some cases, reservoir quality and flow characteristics are totally controlled by diagenesis, as in karsted reservoirs. Some pore systems gain quality as a result of diagenesis. The general trend of pore system quality with time and burial, however, is toward destruction. Certain processes can temporarily interrupt this trend. These are “preserved” pore systems. Some of the processes that preserve pore systems are as follows:

- Reduced burial stress from overpressuring
- Increased rigidity of framework grains
- Oil entry into pore space
- Permeability barriers that isolate the reservoir from fluid flow

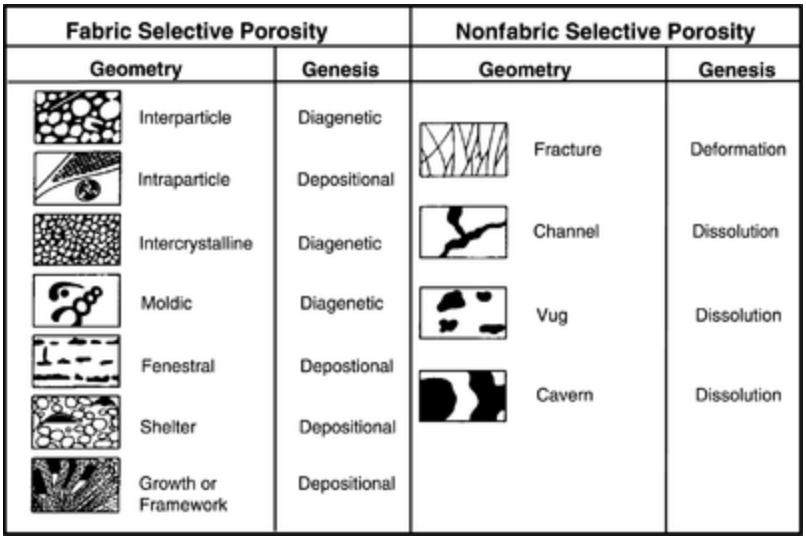

Figure 2.1: Fabric and non fabric pore geometries and processes that create them, from Choquette and Pary (1970).

Predicting reservoir quality in carbonate rocks can be difficult because of the complexity of their pore systems. Applying a combination of concepts of depositional environment, diagenesis, and sequence stratigraphy increases the chances of predicting the quality of reservoir needed for a successful play. There are five basic carbonate depositional environments. From shore to basin, they are peritidal (tidal flat), shallow shelf interior, shelf margin complex, slope, and basin. (F. Jerry, 1993)

The peritidal depositional environment is complex (Figure 2.2). Sediments deposited between mean high and mean low tide are called intertidal sediments, sediments deposited above mean high tide are called supratidal sediments, and sediments deposited below mean low tide are called subtidal sediments. In arid and semi-arid climates, evaporite flats are present from which gypsum and halite are deposited. Eolian sand dunes composed of siliciclastic or carbonate grains may form on the supratidal surface. The shallow shelf interior environment is dominated by low-energy waters that allow lime mud to accumulate. Storms, however, churn the sediment

into suspension, winnowing out the fine-sized material and concentrating the coarse material. Near shorelines, the shelf environment may be composed of offshore bars andspits oriented parallel to shoreline. Shorelines that face heavy wave action accumulate carbonate sand or gravel. Tidal currents are concentrated in channels between islands and produce tidal deltas on the lee side of the island. The shelf margin complex is characterized by the presence of carbonate sands and reefs. Reefs are commonly found at the shelf edge where their rigid framework can withstand strong wave action and they can take advantage of the nutrients upwelling from the deeper waters. Carbonate sands derived from a reef or from plants and animals inhabiting the shelf edge accumulate along a wide belt that follows the break between the shelf edge and the slope. Tidal and storm currents mold the sand belt into tidal channels and bars. The slope is dominated by sediment transport seaward from the shelf margin. Fine-grained sediment settles to the bottom forming thin-bedded mudstones, while slumps, debris flows, and turbidity currents form coarse-grained bodies of breccia, conglomerate, and carbonate sand. The resulting facies patterns depend upon the relief of the shelf margin and the nature of the shallow water portion of the margin. Sediments of the basin environment are dominated by very fine-grained skeletons of planktonic microorganisms, which when lithified, become chalks. They are found in deep basins as well as on drowned shelves.

During the development of F6 gas field in Central Luconia, Wee and Liew (1988) have described the F6 field is a large platform type carbonate buildup, and further divided the field into three lithostratigraphic zones, whereby zone 1 and zone 3 is mouldic limestone with higher porosity than zone 2 which possessed slightly lower porosity with mouldic and chalkified limestone. The study pointed out two uncertainties that would affect the field development which is the possibility of water drive and also the present of tight argillaceous streak that could restrict the vertical flow between zone 2 to zone 3. However, there is still lack of knowledge on the transmissibility of the pores from the three zones that could also impact the field performances.

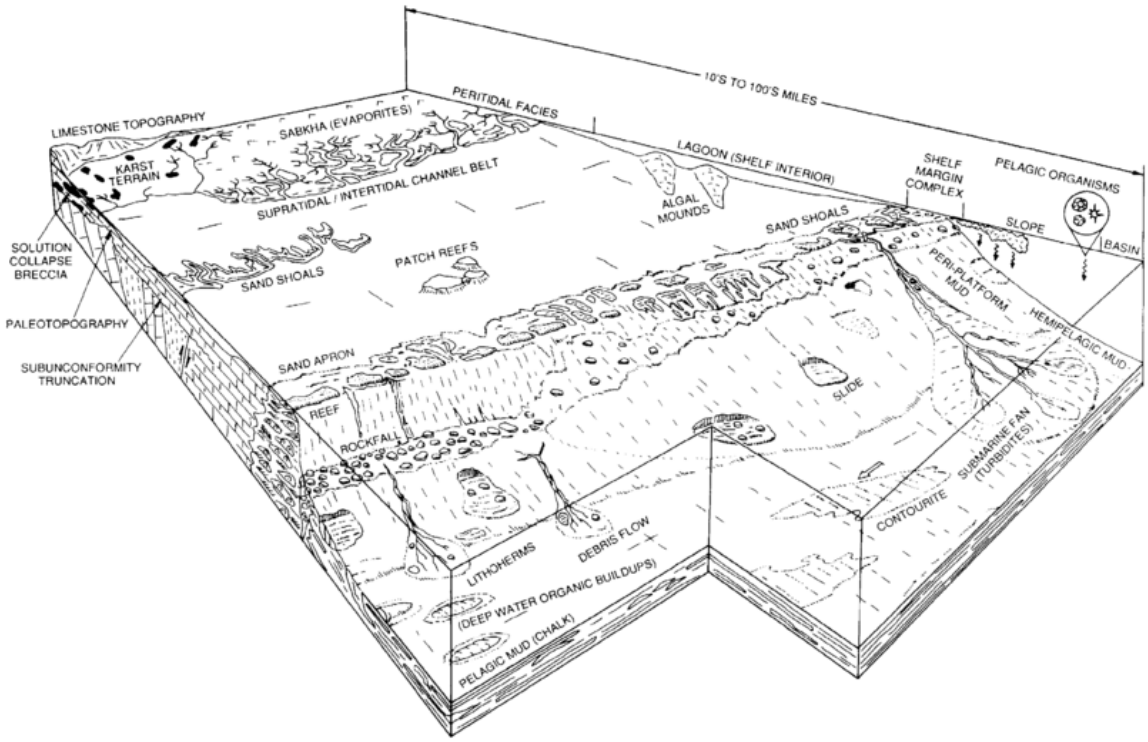

Figure 2.2: Carbonate depositional environment. Diagram by R. G. Loucks and C. R. Handford.

Prior to locate hydrocarbon potential reservoir, pore studies are also essential for the input of petrophysical parameters besides the geological background. In one of the F. Jerry Lucia (1996) paper that studied the petrophysical classification of carbonate pore space for reservoir characterization, he made emphasizes on the importance of vuggy pores as part of the petrophysical parameters for better quantification of geologic models. Further modifying the renowned Dunham (1964) approach of classifying carbonates that itemized packestone into grain dominated or mud dominated. The precise description of the pores is indeed crucial in providing details pore networks information.

On the other hand, Chroqutte and Pray (1970) had also classified the pore types into fabric selective and non-fabric selective. They have understood the relation between the pore space and fabric elements of carbonate facies ranges from complete dependence, as for primary interparticle porosity, to complete independence, as for tectonic fractures in nonporous limestone. If a dependent relation can be discerned between porosity and fabric elements, it is referred that the porosity as fabric selective. If such relation cannot be established, it is classified that the porosity is non fabric selective. In fact, fabric

selectivity is especially useful in determining the origin of pores in relation to other events in the diagenetic evolution and thus, the pore behavior.

Carbonate reservoir descriptions are based on observations of depositional and diagenetic fabrics and pore space from core and cuttings samples. The descriptions are correlated with wireline log responses and incorporated into geological facies and/or diagenetic models in order to map porosity, water saturation, and permeability.

There exists a range of methodology to extract networks from pore space images. However, using an integrated approach that allows the reconstruction and prediction of 3D pore structure modifications and porosity/permeability development throughout carbonate diagenesis has become widely common. Reactive Pore Network Models (PNM-R) done by researchers E. De Boevercan et.al (2012) can predict changes in the transport properties of porous media, resulting from dissolution/cementation phenomena. The validity and predictability of these models also depended on the representativeness of the equivalent pore networks used and the diagenetic events occur on the place of interest. A comparative study of different micro-CT network extraction methods (medial axis, maximal ball, velocity based, grain recognition based algorithms) has also been reviewed by Hu Dong et.al (2008) with two carbonates and one sandstone samples showing the favorable and unfavorable condition of the model based on several simulations and the pore skeletons capture by CT scanners.

Thermal conductivity (k) is the property of a material to conduct heat. Heat transfer occurs at a higher rate across materials of high thermal conductivity than across materials of low thermal conductivity. There are several a few influencing factors that would affect the thermal conductivity property of carbonate rocks, in relation to the density, crystal structure, grain contact and chemical composition of the minerals (Horai, 1940). Generally, rocks with higher porosity will have lower thermal conductivity due to its loosely packed grains and the medium of heat transfer is mainly through air rather than the matrixes or minerals in the rocks. On the other hand, theoretically, rocks with lower porosity will have higher thermal conductivity.

CHAPTER 3

METHODOLOGY

3.1 Project Flow

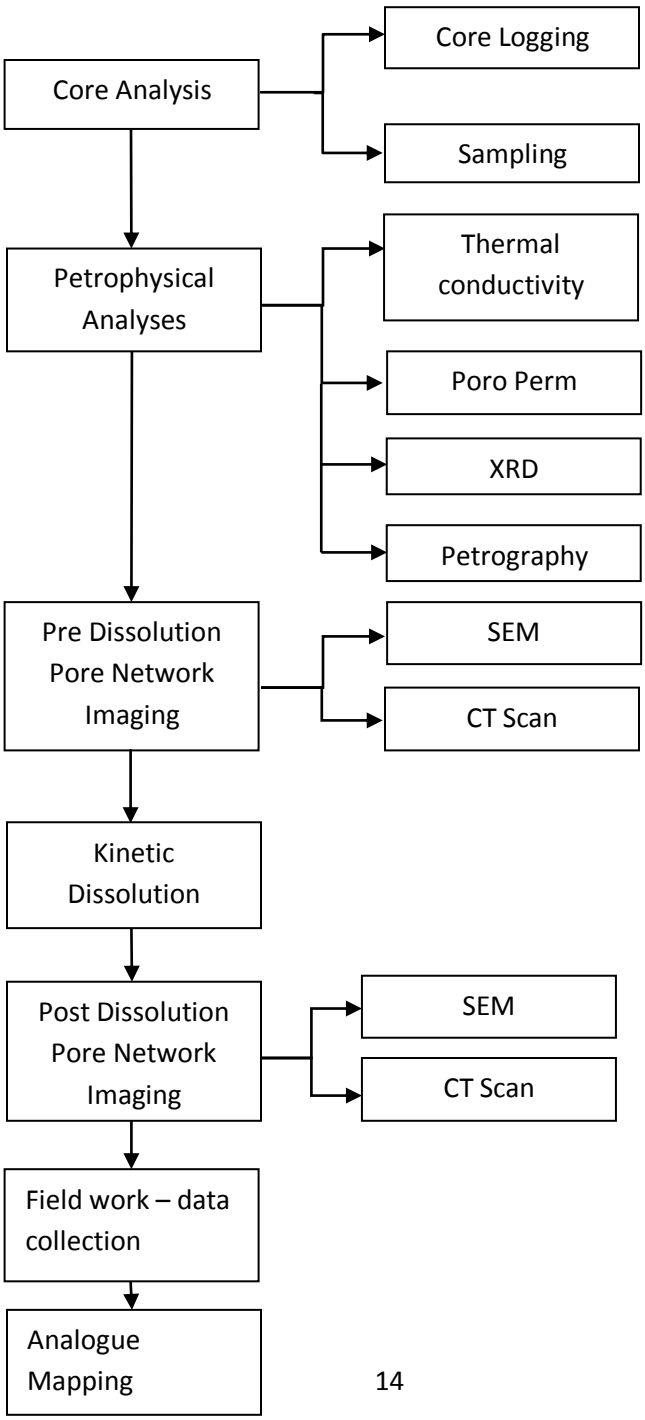

3.2 Gantt chart (Table 1)

No	Project Activities	1	2	3	4	5	6	7	8	9	10	11	12	13	14	15	16	17	18	19	20	21	22	23	24	25	26	27	28
1.	Proposing Title																												
2.	Selection of Project Topics																												
3.	Preliminary Research Work																												
4.	Core Lab Visit																												
5.	Core Analysis/ Lab Tests																												
6.	Proposal Defense/ VIVA																												
7.	Field Visit/ Mapping																												
8.	Submission of Reports																												

Key Milestone

3.3 Methods/ Analysis

Petrophysical Analyses

Core Logging/ Core Analysis

Two cores from both wells were logged manually and core description was done carefully by using a standard carbonate manual that describes and classifies each facies with the following details depth, lithology, composition, porosity, permeability, texture, strata/ Bedding, post depositional features, color and fossils/ mineral. The data were then digitized into lithology logs that represent the real cores by using Sedlog software.

Thermal Conductivity

Thermal tests were done on four core samples (previously identified facies from core logging). Heat were given to one side of the cylindrical core's surface at H=40 from the power source across the length of 8cm depending on samples availability. Temperature differences were obtained from electronic thermometer with two metal probes that measure temperature from the heat origin and the other end of the sample across the length. Thermal conductivity (k) was then calculated based on the equation shown below:

$$Q = kA\frac{T1-T2}{L}$$

Where,

H= Heat
K= Thermal Conductivity
A= Area
L= Length
T= Temperature

XRD (X-Ray Diffraction) Analysis

XRD were done on the 10μm powdered rock samples where copper (Cu) was used as the standard wavelength. The X-ray diffraction (XRD) patterns were recorded with a SIEMENS D5000 diffractometer. The diffractometer was equipped with a Ge-focusing primary monochromator giving Cu-Kα radiation (λ = 1.5406 Å). Minerals detected from the samples were recorded in peaks and then analyzed with PowderX software.

PoroPerm Analysis

POROPERM instrument combines both permeameter and porosimeter that determines properties of core plugs with 1 inch diameter under 400 psi confining pressure by injecting inert gas and slowly releasing the pressure until it dropped to zero. Porosity, Klinkenberg permeability, bulk density, voids volume and etc. were then directly produced.

Petrography Analysis (Thin Section)

Seven samples were initially vacuum-impregnated with blue-dyed epoxy resin to assist recognition of porosity. Thin section was then prepared from the blue-dyed samples through several repeated procedure of cutting, trimming and also polishing using GEOCUT cutter, GEOFORM precision cutter and FORCIPOL 300-1Vgrinding and polishing machine with speed of 100rpm respectively.

The thin sections were then analyzed with a petrographic polarizing microscope equipped with high resolution digital camera to describe the quantitative and qualitative analyses, including comments on texture, porosity, pore types and mineralogy.

Pore Network Imaging

FE-SEM (Field Emission Scanning Electron Microscope) Analysis

This analysis was done with a LEO-6VP1430 scanning electron microscope unit with operating conditions ranging from 10 to 15 kV accelerating voltage. SEM images were captured at magnification from 200x to1000x. EDX were conducted with detection limits ranging from 100-0.1 wt %.

Computed Tomography (CT) Scanning

Four samples were scanned with inspeXio SMX-225CT scanner to obtain the 3D view of the pore network with following specifications for the X-ray generator and detector. Images obtained were rendered using the VG Studio and Pro Image Analyzer software to acquire the pore throat connectivity, volume porosity (3D) and area porosity (2D).

X-Ray Generator: Non – enclosure tube type rated power: 135W

: maximum tube voltage: 225kV

: maximum tube current: 1000µA

X-Ray Detector: Image intensifier or flat panel detector

Kinetics Dissolution

Dissolution

This experiment was to testify the changes of the pore network after dissolving the samples with 0.01mol hydrochloric acid solution over a period of time at room temperature. The initially weighted rock samples were dipped into a minute amount of hydrochloric acid (HCl) in a beaker and then laid on a stirrer for 5minutes. After drying the samples, the weight loss was recorded to determine the amount of rock dissolved. The same step was repeated for 12times, with each time increment of 5mins. The acid used to dissolve the rocks was collected for further atomic absorption spectrometry (AAS) analysis.

The recorded weigh loss was then plotted into a graph of absolute weight loss versus time and cumulative weight loss versus time to examine the weight loss trend and then the rate of dissolution was calculated based on the following equation:

$$rate = \frac{total\ weight\ loss(g)}{total\ time(\text{min})}$$

Atomic Absorption Spectrometry (AAS) Analysis

In this study, the technique is used for determining the concentration of calcium and magnesium dissolved in the hydrochloric acid (HCl) after dissolution of the rock samples. Total of 48 liquid samples were collected throughout the dissolution process and each of them were tested for both calcium and magnesium concentration. Dilution was done beforehand due to the high concentration of calcium and magnesium content in the liquid samples. The standard concentrations used to calibrate the equipment were 5ppm, 10ppm, 15ppm and 20ppm. The rate of dissolution was calculated based on the following equation:

$$rate = \frac{total\ concentration\ of\ Ca/Mg(ppm)}{total\ time(\text{min})}$$

CHAPTER 4

RESULTS & DISCUSSION

4.1 Core Data

Core Logging Well F4-1

Well F4-1 has a total length of approximately 5.7m of core. Three distinctive facies (Facies 4A, 4B and 4C) has been identified according to their distinctive sedimentary features. The facies were named alphabetically according to their depth, with Facies 4A located at shallowest depth, followed by Facies 4B and 4C. Basically, Facies 4A was similar to Facies 4C but separated by Facies 4B in between, thus there was only two different types of facies identified within well F4-1. The stratigraphic log below (Figure 4.1) shows the overall logs of the well F4-1 with symbols displaying the sedimentary features, lithology type and also fossils found within the well.

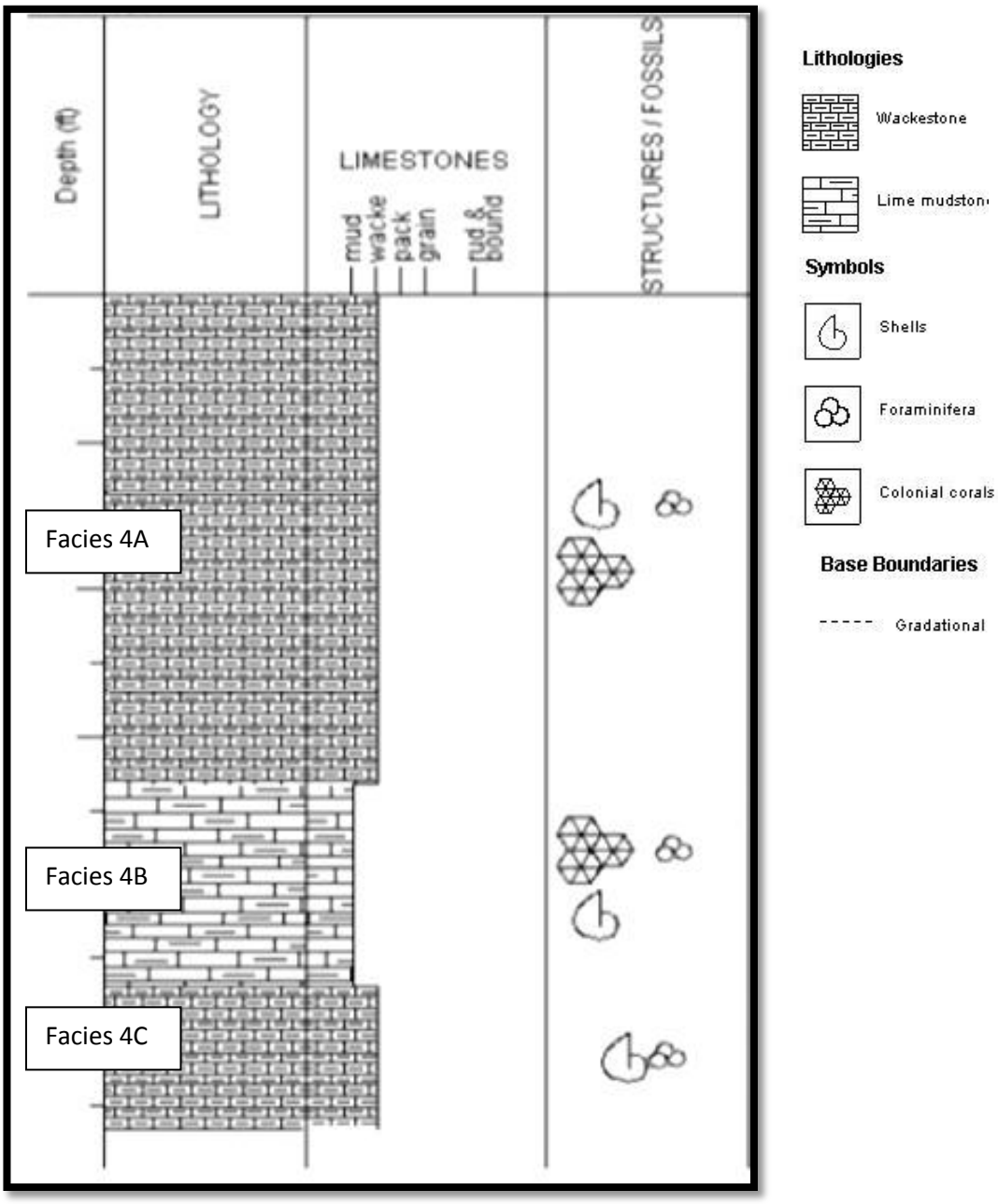

Figure 4.1: Stratigraphic log of Well F4-1.

(b) Core Description Well F4-1

Facies 4A

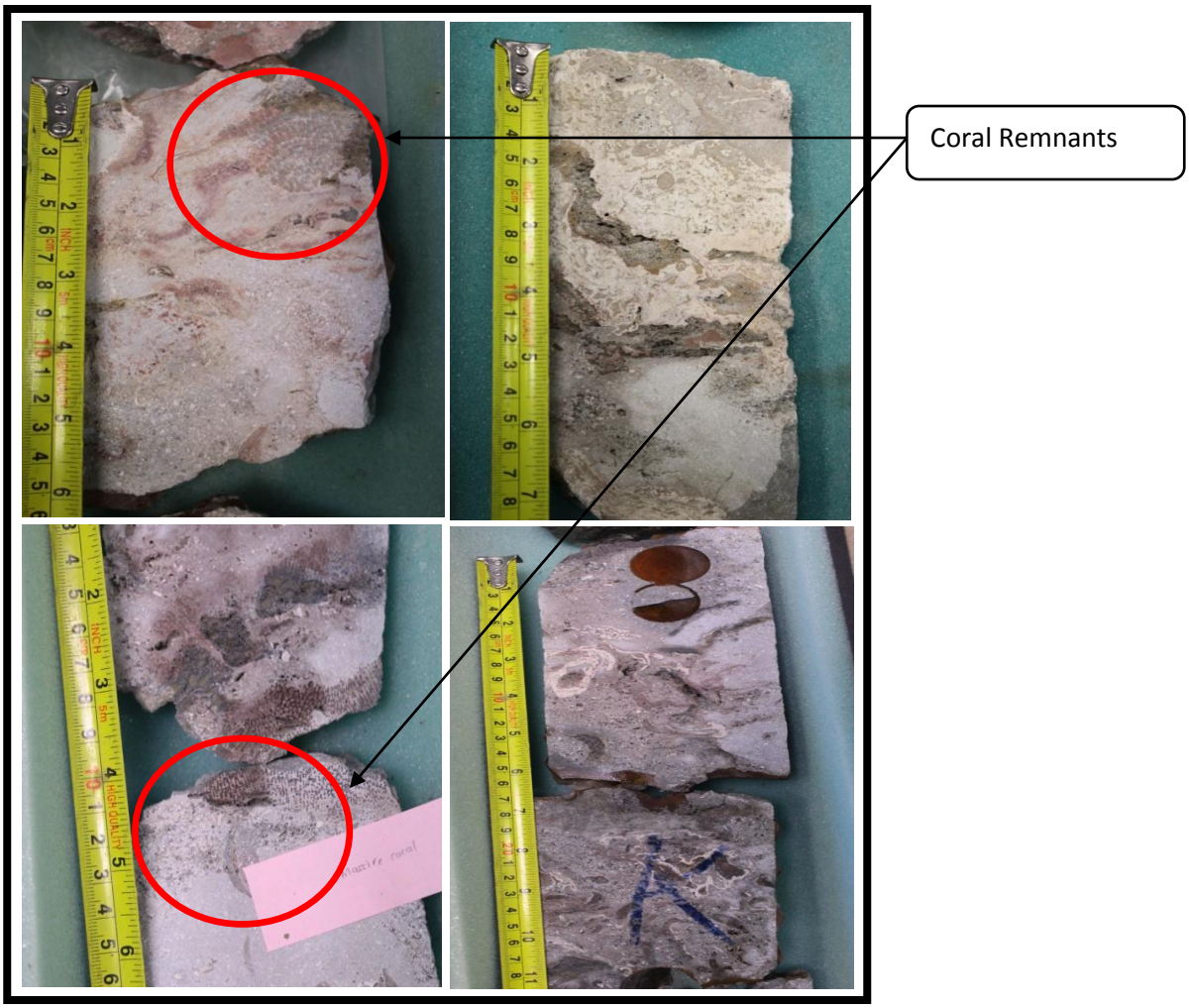

Figure 4.2: Sedimentology core from facies 4A.

Facies 4A with length about 3.3m is limestone categorized with its massive bedding and obvious ferum deposits (which do not react with acid) within the limestone that makes the reddish-grey color to the core. The mud supported core is possessed of microfossil deposits like foraminifera and white caliches binding within the mud. Occasional massive coral remnants (red circles) are also observed binding within the mud. Porosity in this facies is considered fairly high because there are many visible millimeter pores and vuges larger than 5cm at some intervals. The grains are consolidated and fairly tight.

Facie 4B

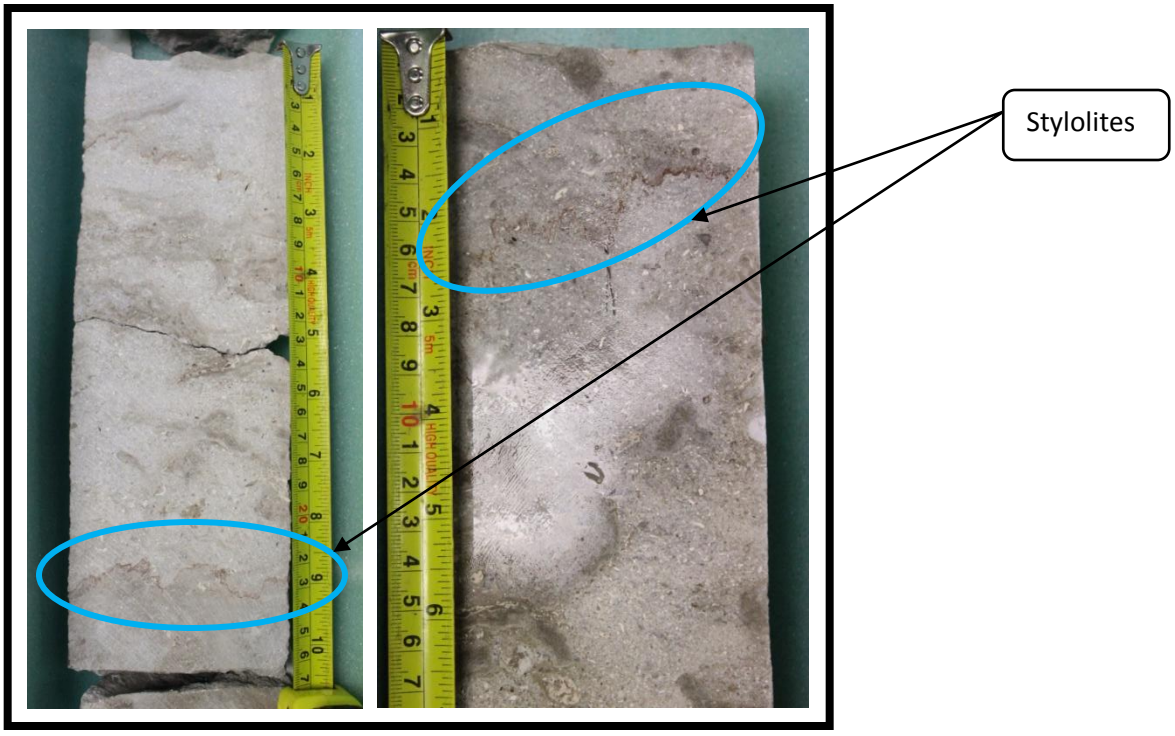

Figure 4.3 : Sedimentology core from facies

Facies 4B with length about 1.4m is limestone characterized with the tightly consolidated grain and lower porosity. Mainly mud supporting texture mudstone with abundant presence of microfossils. Massive bedding with gradual decrement in porosity from the previous facies. Distinctive stylolite features (blue circle) are observed at some intervals. Greenish grey in color.

Facies 4C

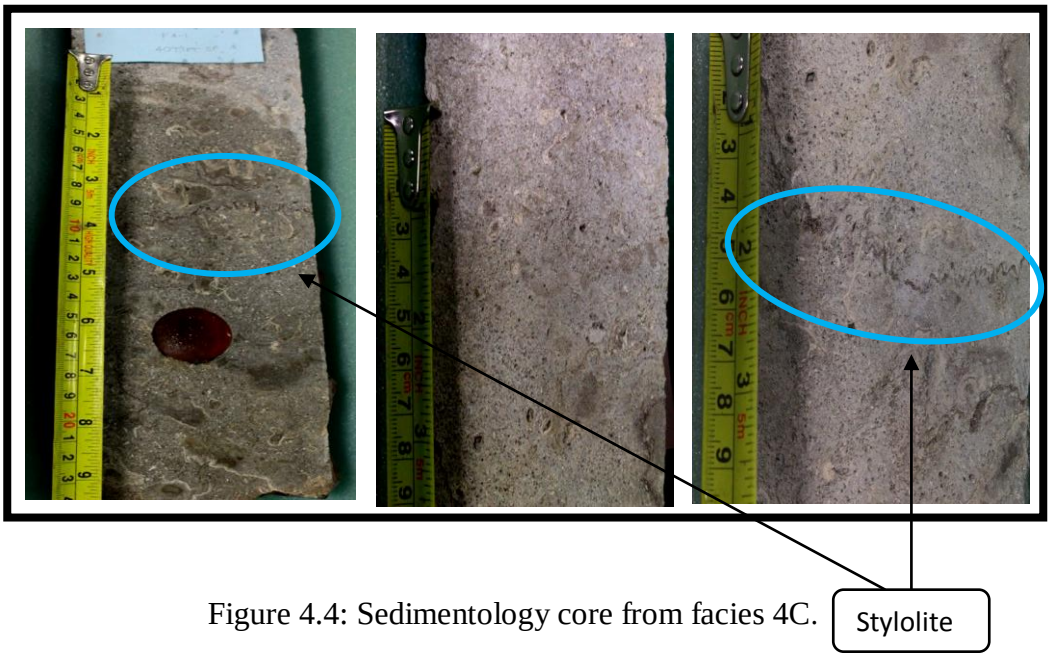

Figure 4.4: Sedimentology core from facies 4C.

Facies 4C with length of approximately 1m is limestone characterized with its fairly high porosity (pores larger than 5mm) and lightly consolidated mud supporting wacky texture. Obvious caliches and oncoids? are observed at close intervals, stylolite feature (blue circle) is seen too. Abundant of microfossils are found within the core. Dark grey in color.

(a) Core Logging Well F6-1

Well F6-1 has a total length of approximately 15m of core. There was only one sucrosic facies being identified throughout the cores and has been named as Facies 6A. There were no visible sedimentary features and fossils content visible within the core.

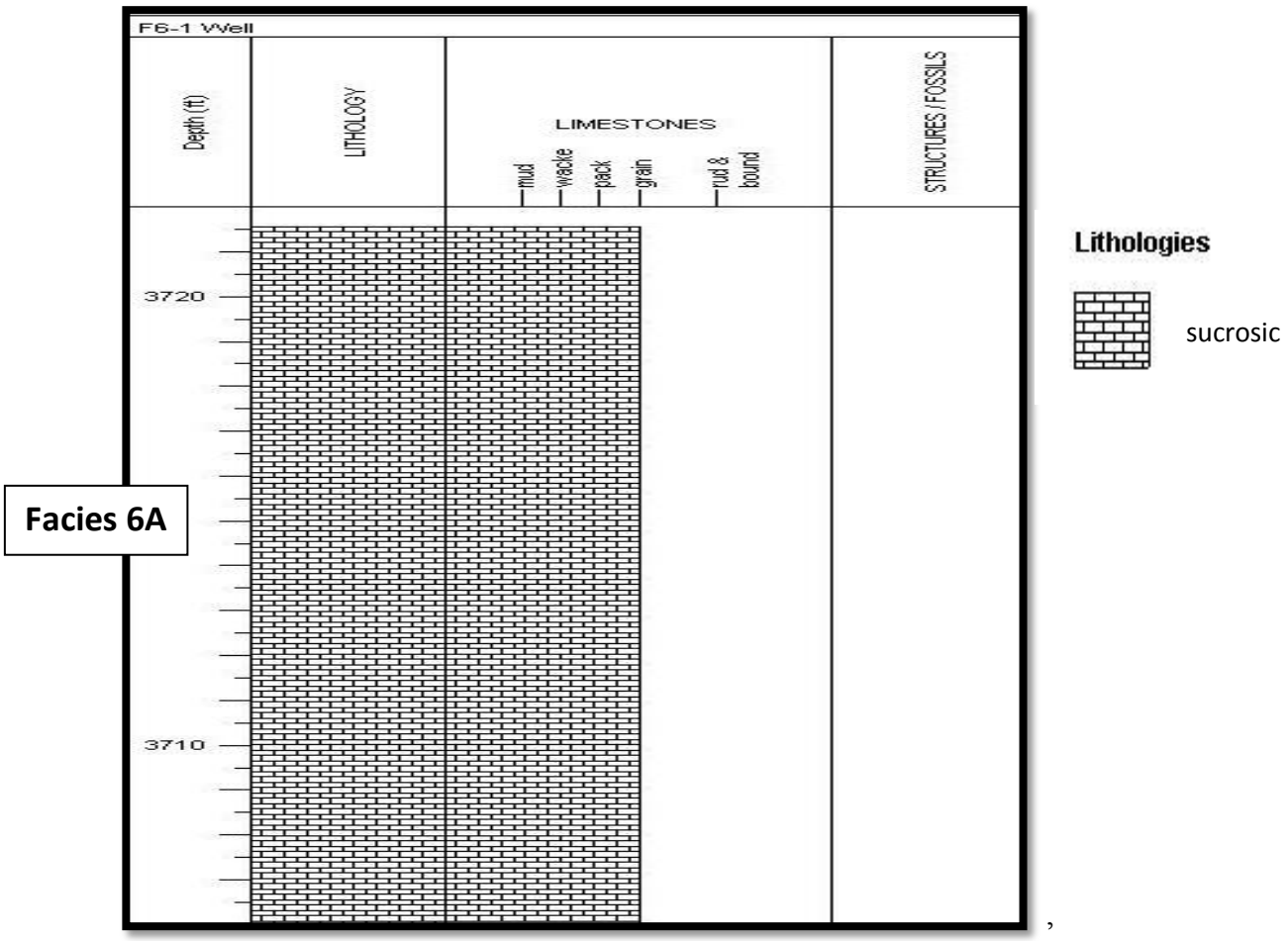

Figure 4.5: Stratigraphic log of Well F6-1.

(b) Core Description Well F6-1

Facies 6A

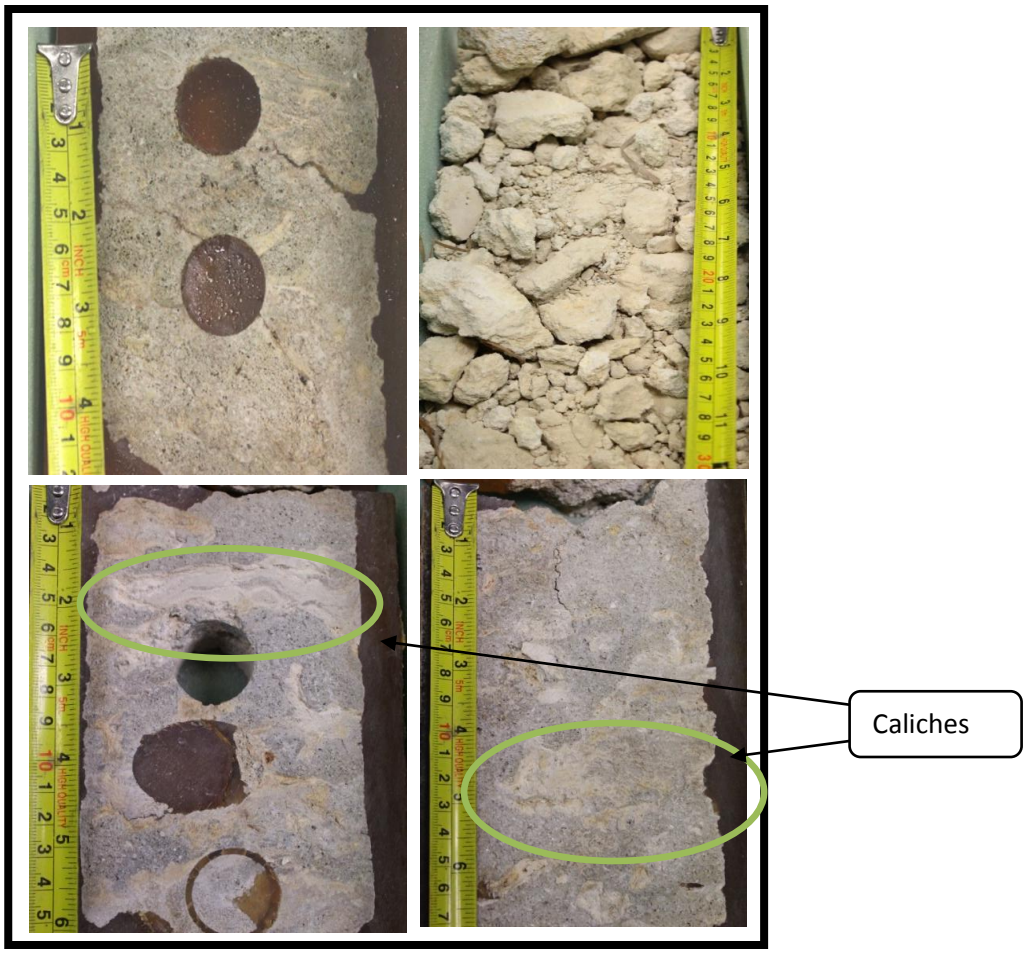

Figure 4.6: Sedimentology core from facies 6A.

Facies 6A is monotonous carbonate limestone throughout the 15m core with its very fragile and sucrosic texture. The core was porous and very slightly undurated, where most of the core were in debris. There was some litho clast observed that giving out faint reflectivity from the crystals within the core. No obvious bedding differences within the 15m core and no skeletal fragments were observed. There were major caliches (green circle) infill within the core. Light grey in color.

In its entirety, albeit both wells were drilled at the same F filed of the Central Luconia carbonate platform, it is observed that both wells are possessing rather distinctive lithology. This is interpreted that, the two wells drilled were at different location of the rimmed carbonate platform. The F4 well is believed to drill at the fore slope of the platform and possessing the fore reef facies, because of its chaotic mixture of many features within the vertical well. This area acts as sink for excess carbonate sediment: most of the sediment produced in the lagoon and reef is transported by various processes and accumulates in the slope. Therefore, the slope contains coarser sediments than the reef and lagoon. That is evident enough to explain the fairly high porosity in this well and also the coral remnant binding within the carbonate matrix. With the amount of foraminifera and other microfossils found within this facies, it is interpreted that environment of deposition for the F4 well was warm shallow water, right in front of the rim of the platform, where most of the carbonate sediments could be deposited and for carbonate microfossils to survive. However, as aforementioned, carbonate are very prone to diagenesis, patchy diagenesis could add to the impression of almost chaotic diversity and irregularity. As the carbonate was deposited at the age of mid Miocene, diagenesis could have altered the originally deposited features e.g. compaction or recystallization would have decreased the primary pores. Similar event could have happened to the F6 well, due to its heavily altered texture, which is interpreted to have undergone severe recrystallization into coarser crystals grain and most of the primary carbonate features had been wiped out from sight with no trace of fossils or any other reef remnant. The exact location of the F6 wells was not certain due to the destructive evidence about the origin of the carbonate deposition. However, instead of pore minimizing, it is interpreted that the post dissolution diagenetic events has enhanced the porosity of the wells with even pore distribution throughout the cores.

4.1 Petrography Analysis

Facies 4A

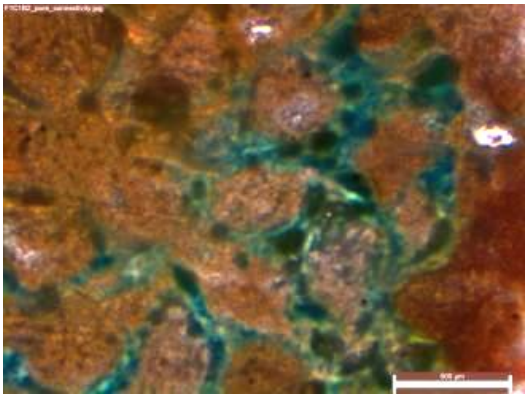

Figure 4.7: Pore connectivity of Facies 4A.

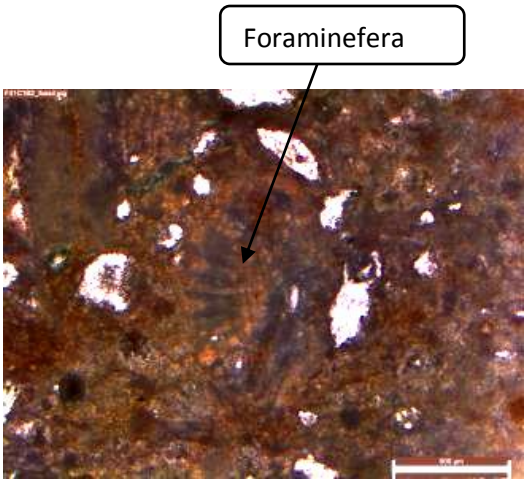

Figure 4.8: Foraminifera from Facies 4A.

Petrography analysis in Facies 4A has shown that the pore connectivity was pretty good as shown in figure 4.7 (blue stain). It shows that the pore type possessed by Facies 4A were mainly from connected pores of about 500µm in length. The connected pores could be formed by connecting micro fractures or the mouldic coral net-like structure. Other than that, intact benthic foraminifera (unidentified species) of about 500µm in size was observed too under the microscope. This has indicated that the depositional environment of the facies was favorable for fossil preservation.

Facies 4B

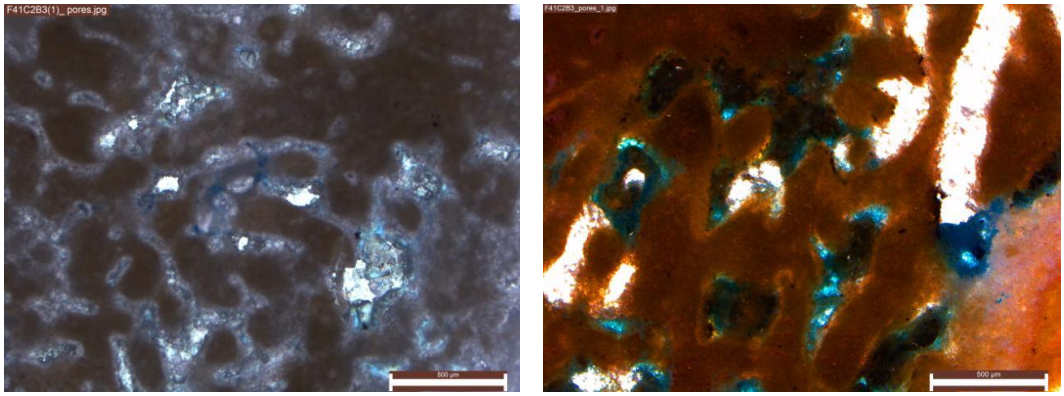

Figure 4.9: Pore network in Facies 4B.

Facies 4B displayed excellent pore connectivity under microscope with typical coral mouldic pore type. Pore throat of about 50µm in length. No significant fossils were found.

Facies 4C

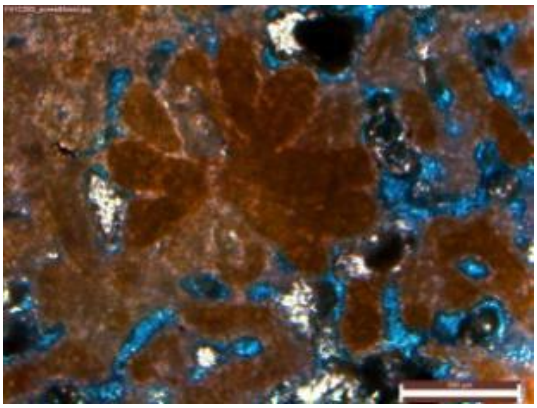

Figure 4.10: Pore network of Facies 4C.

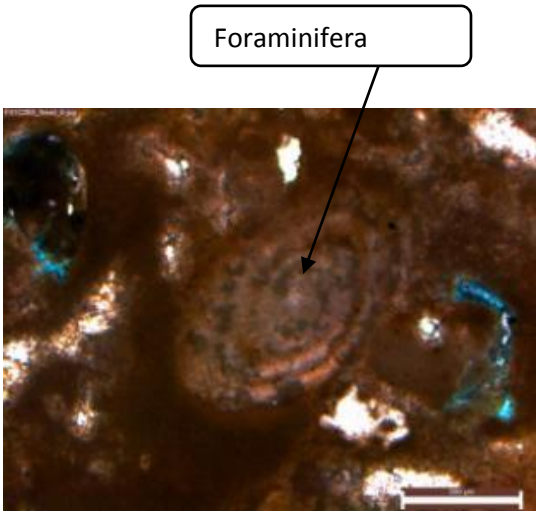

Figure 4.11: Foraminifera of Facies 4C.

Pores in Facies 4C has shown mouldic pore type with coral structures (blue stain). This has established excellent connectivity between the pores with pore throat about 100µm in size. Foraminifera of unidentified species, about 600µm is size was found as well.

Facies 6A

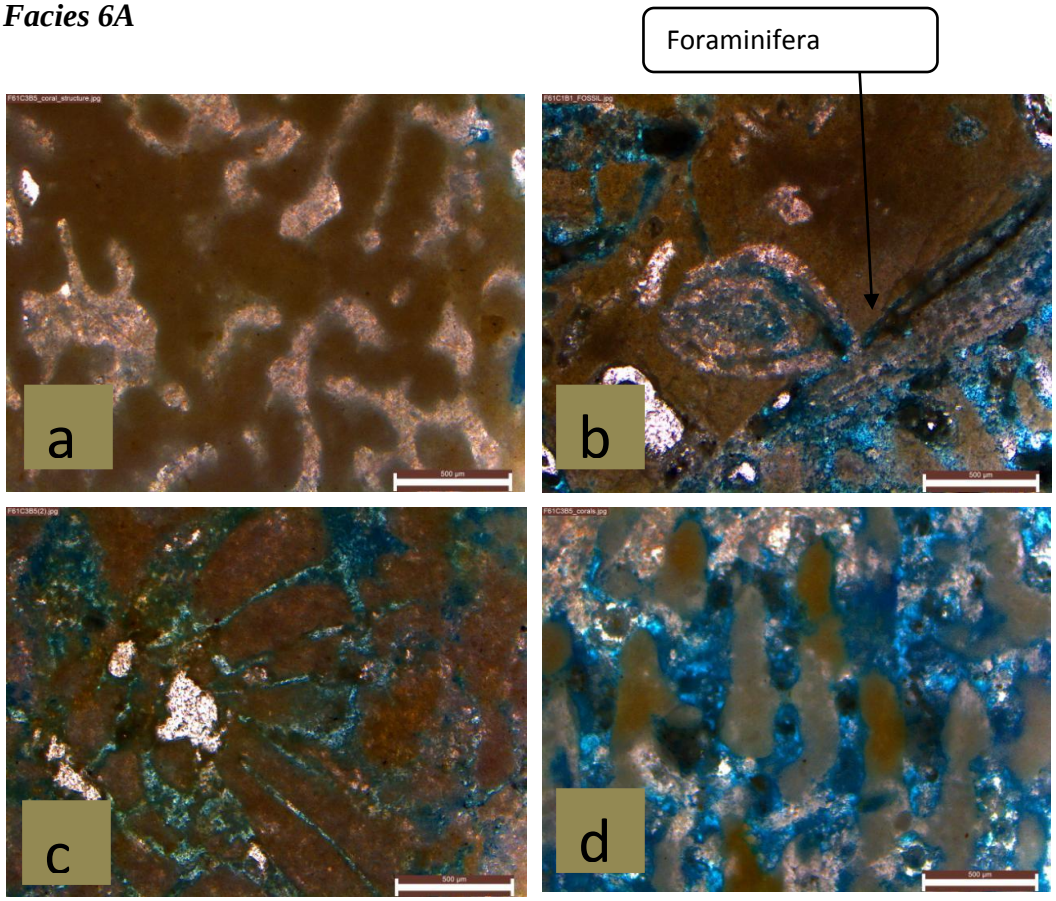

Figure 4.12: (a), (d) showing pore connectivity and coral mouldic pore type of Facies 6A. (b) foraminifera. (c) Possible micro fracture?

Facies 6A albeit has little observation of coral remnants from the core analysis, but it was obvious under microscopic analysis, where most of the pores associated in well F6-1 were from the coral structures. As compared to well F4-1, the coral structures here were more loosely packed and thus, having pore throat about 150µm in length, which was slightly bigger than the F4 well. There was a possible micro fracture as depicted in figure 4.12c. Generally, the connectivity of the pores was excellent, as shown in figure 4.12 that all the pores are interconnected without any prominent isolated pore. On top of that, intact foraminifera was found too (Figure 4.12d) and showing another mouldic pores where the fossils has been dissolved leaving it porous (blues stain within the fossil).

4.2 Poroperm Data

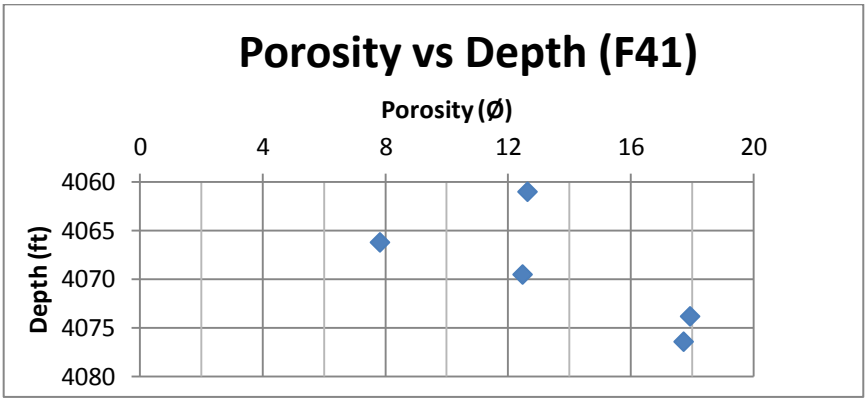

Figure 4.13: Porosity versus depth graph of the F4 well.

Porosity versus depth graph of the well F41. The distribution of porosity was unusual where deeper facies having higher porosity than the shallower facies, suggesting possibilities that the deeper facies might be more prone to diagenetic events than the shallower facies. Or perhaps the shallower facies have gone through recrystallization and having more tightening pores.

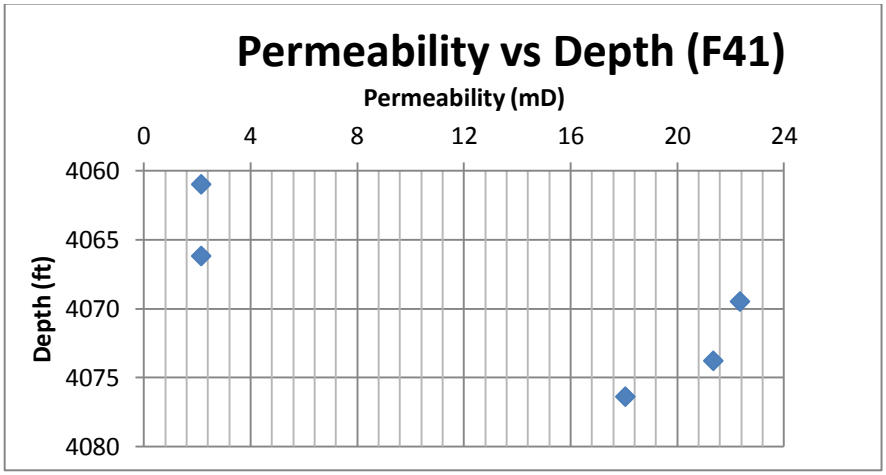

Figure 4.14: Permeability versus depth graph of the F4 well.

Permeability versus depth graph of the well F41. The permeability distribution tallies well with the given porosity albeit the unusual trend. Whereby, facies with higher porosity were possessing higher permeability and vice versa.

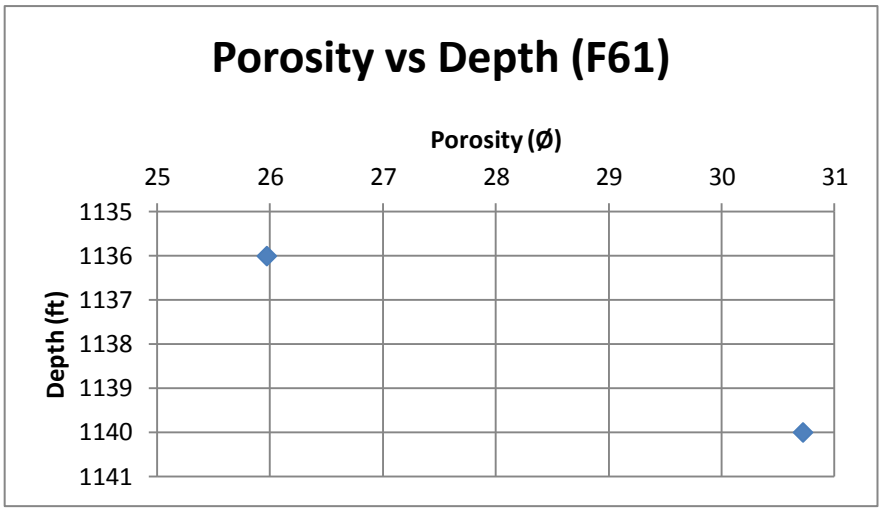

Figure 4.15: Porosity versus depth graph of the F6 well.

Porosity versus depth graph of the well F41. The points showed that shallower facies have lower porosity compared to the deeper facies. Suggesting the similar possibilities as stated in F41 well too. It could be the deeper facies had undergone diagenetic events that enlarged the pores or the shallower facies had undergone diagenetic events that shrunk the pores.

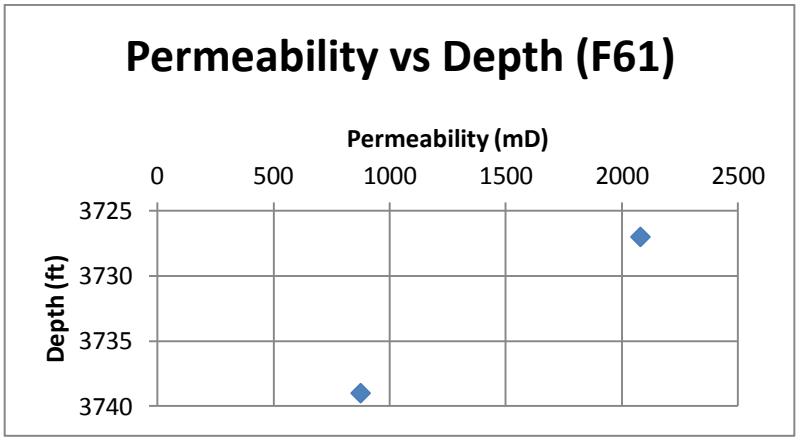

Figure 4.16: Permeability versus depth graph of the F6 well.

Permeability versus depth graph of the well F41. Results from permeability suggests that the shallower facies albeit having low porosity but showing high permeability of approximately 2000mD, whereas the deeper facies permeability was only 900mD of permeability albeit the high porosity.

4.3 Energy Dispersive Using X-Ray (EDX) Data

Table 2: EDX data of the pores examined from F4 and F6 well.

Sample Name	Element	Weight %	Atomic %	SEM of EDX
F41C2B1 Pore1/ Point 1	C K O K Mg K Ca K	17.62 56.28 9.54 16.56	25.33 60.76 6.78 7.14	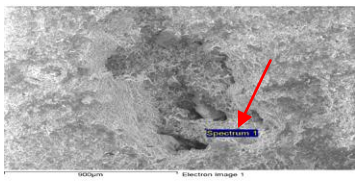
F41C2B1 Pore1/ Point 2	C K O K Mg K Al K Si K Ca K	17.37 50.93 9.60 1.09 0.39 20.60	25.85 56.93 7.06 0.72 0.25 9.19	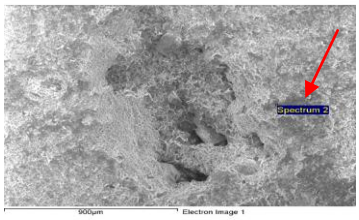
F41C2B1 Pore1/ Point 3	C K O K Mg K Si K Cl K Ca K Br L	12.43 52.29 9.98 0.82 0.32 23.05 1.10	19.38 61.19 7.69 0.55 0.17 10.77 0.26	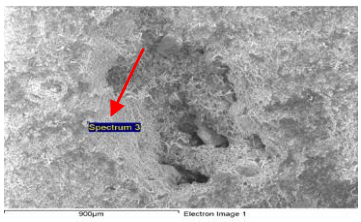
F41C2B1 Pore2/Point1	C K O K Mg K Ca K	15.17 53.00 1.83 30.00	23.39 61.36 1.39 13.86	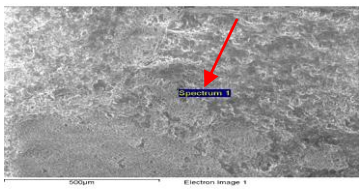
F41C2B1 Pore2/Point2	C K O K Mg K Al K Ca K	16.45 49.69 9.74 0.36 23.77	24.98 56.65 7.31 0.24 10.82	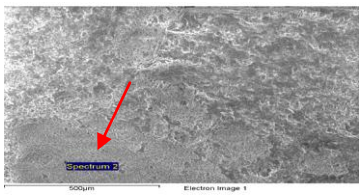

F41C2B1 Pore2/Point3	C K O K Mg K Si K Cl K Ca K	4.03 49.25 2.73 0.59 0.54 42.85	7.25 66.46 2.43 0.46 0.33 23.08	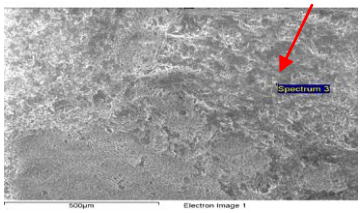
F41C2B1 Pore3/Point1	C K O K Mg K Si K Ca K	25.11 46.60 7.17 0.55 20.57	35.85 49.95 5.06 0.33 8.80	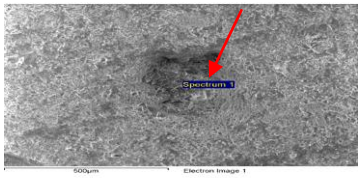
F41C2B1 Pore3/Point2	C K O K Mg K Si K Ca K Br L	18.33 51.43 8.63 0.42 20.45 0.75	27.10 57.10 6.30 0.27 9.06 0.17	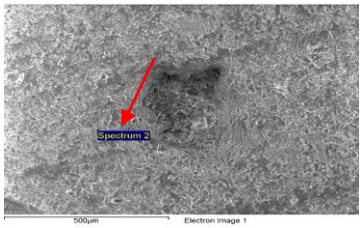
F41C2B1 Pore3/Point3	C K O K Mg K Si K Ca K	16.97 51.66 10.38 0.46 20.54	25.24 57.69 7.63 0.29 9.16	
F41C2B1 Pore3/Point4	C K O K Mg K Ca K	15.34 47.85 10.81 26.00	23.82 55.97 8.29 12.10	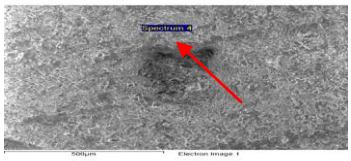
F41C2B1 Pore4/Point1	C K O K Mg K Ca K	29.60 45.07 5.38 19.95	41.07 46.95 3.69 8.30	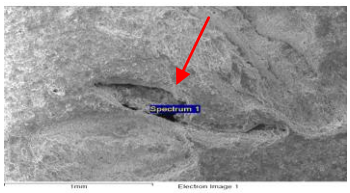
F41C2B1 Pore4/Point2	C K O K Mg K Ca K	15.43 54.75 1.31 28.51	23.48 62.54 0.99 13.00	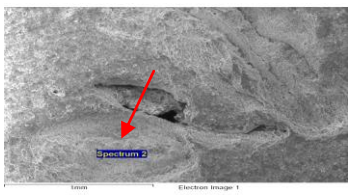

F41C2B1 Pore4/Point3	C K O K Mg K S K Ca K	22.30 46.71 7.92 0.62 22.45	32.68 51.39 5.74 0.34 9.86	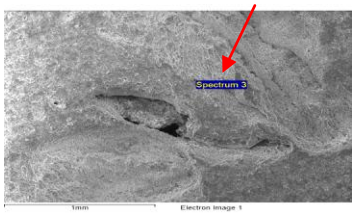
F41C2B1 Pore4/Point4	C K O K Mg K Ca K	28.36 45.16 4.21 22.27	39.93 47.74 2.93 9.40	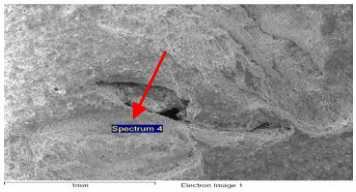
F41C2B6 Pore1/Point1	C K O K Mg K Ca K	36.45 38.86 4.01 20.68	49.39 39.53 2.68 8.40	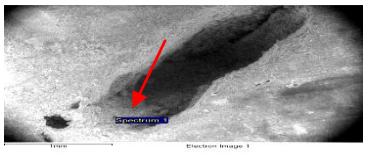
F41C2B6 Pore1/Point2	C K O K Mg K Al K Ca K	12.87 49.40 5.67 0.45 31.61	20.61 59.41 4.48 0.32 15.17	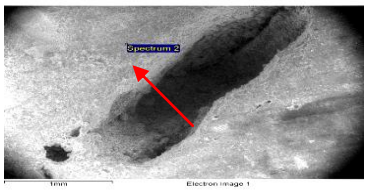
F41C2B6 Pore1/Point3	C K O K Mg K Si K Ca K	16.64 55.90 9.57 0.67 17.22	24.19 61.02 6.87 0.42 7.50	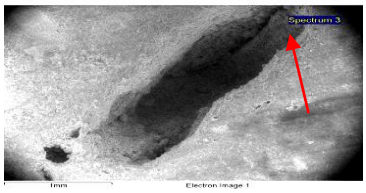
F41C2B6 Pore1/Point4	C K O K Mg K S K Ca K	28.75 43.47 6.03 0.64 21.11	40.54 46.01 4.20 0.34 8.92	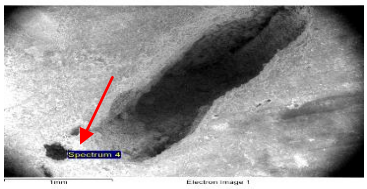
F41C2B6 Pore2/Point1	C K O K Mg K Si K Ca K	18.30 55.64 8.52 0.44 17.09	26.29 60.03 6.05 0.27 7.36	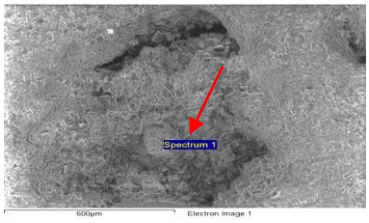

F41C2B6 Pore2/Point2	C K O K Mg K Ca K	13.14 49.36 7.72 29.77	20.88 58.88 6.06 14.18	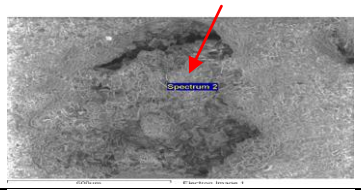
F41C2B6 Pore2/Point3	C K O K Mg K Ca K	16.13 53.02 10.33 20.53	24.00 59.24 7.60 9.16	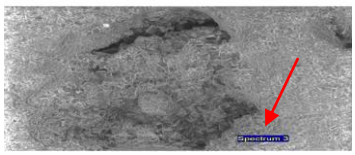
F41C2B6 Pore3/Point1	C K O K Mg K Ca K	21.73 47.31 5.85 25.11	32.12 52.49 4.27 11.12	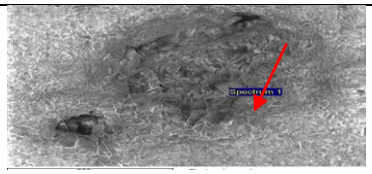
F41C2B6 Pore3/Point2	C K O K Mg K Ca K Br L	19.44 42.86 4.69 31.96 1.06	30.53 50.54 3.64 15.04	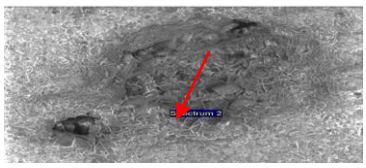
F41C2B6 Pore3/Point3	C K O K Mg K Al K Ca K	15.43 55.97 9.12 0.30 19.18	22.75 61.94 6.64 0.20 8.47	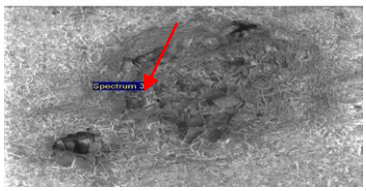
F41C2B6 Pore3/Point4	C K O K Mg K Si K Ca K	23.53 49.27 5.71 0.60 20.89	33.69 52.95 4.04 0.37 8.96	

EDX result showed that most of the pores are made up of element calcium, oxygen, magnesium, silica and also carbon. There is occasionally barium, sulphur and aluminum exists in some of the pores as well. However, statistic shows that carbon, calcium, magnesium and oxygen are the most abundant element found around the pores, which very much indicating and supporting the idea that the samples are made up of the two major carbonate mineral – calcite and dolomite.

4.4 Scanning Electron Microscope (SEM) Images

Facies 4C

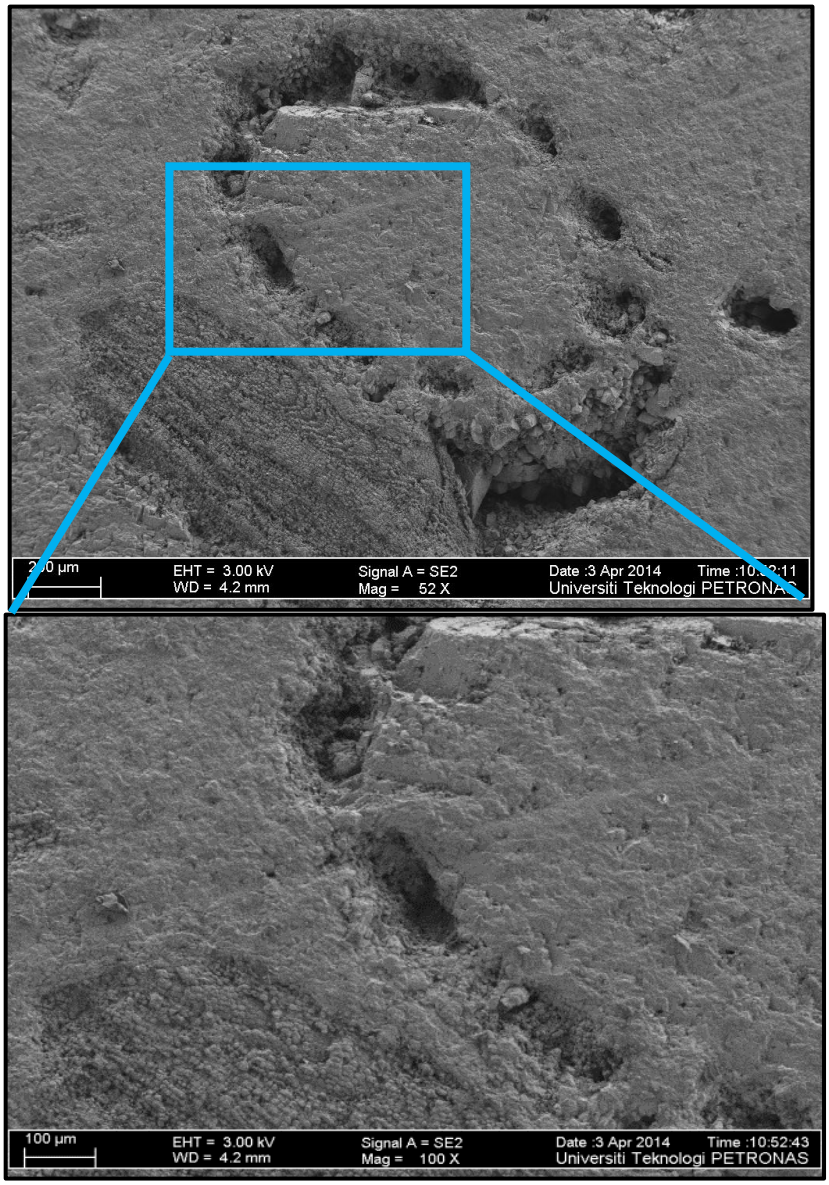

Figure 4.17: SEM images of one of the pores from facies 4C BEFORE dissolution. Showing circular ring of pores at magnification of 52x, high chance of low bonding material about 200µm in diameter. Zoomed in one of the pores showing low crystallization within the pores at magnification 100x.

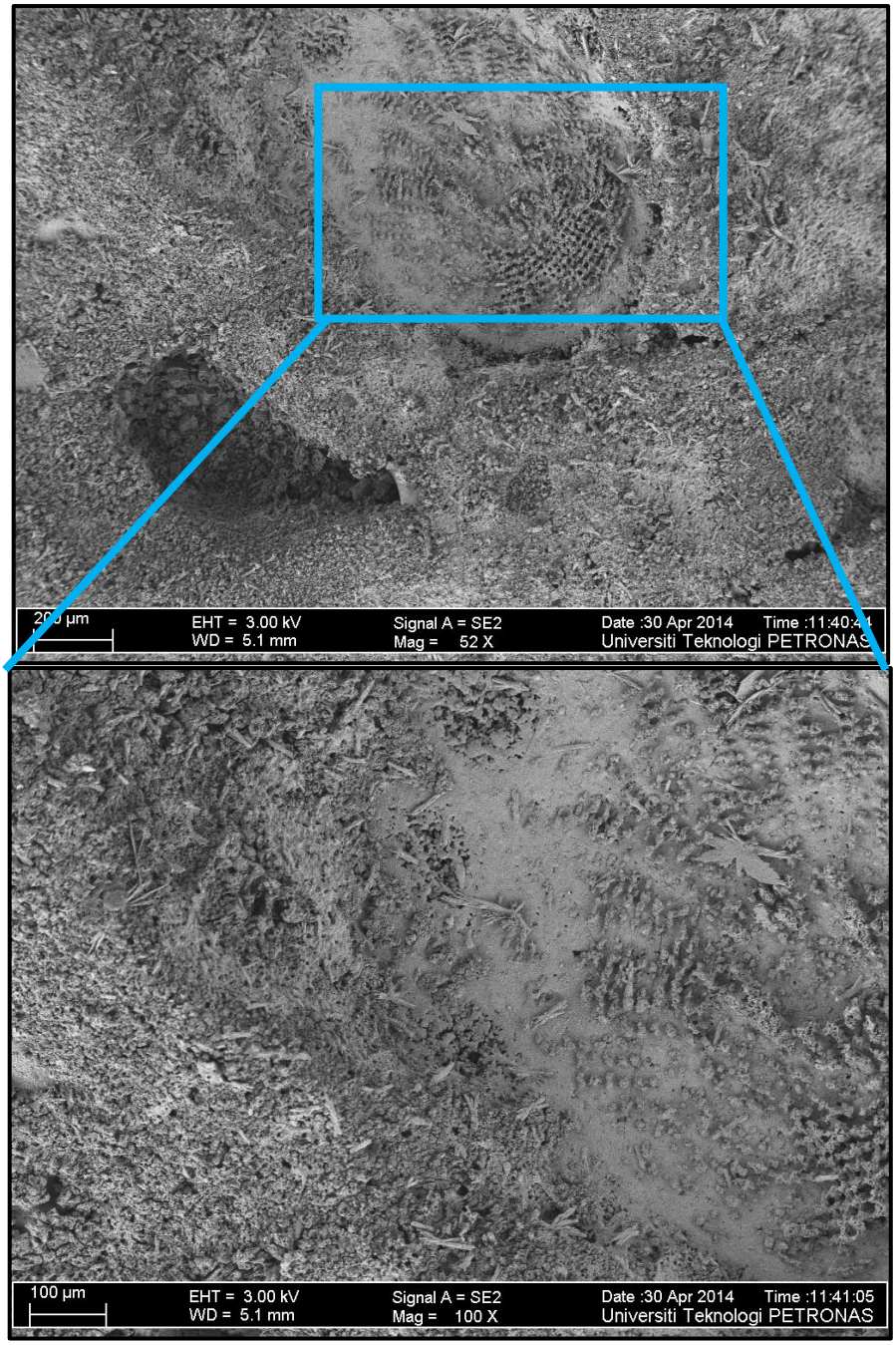

Figure 4.18: SEM images showing one of the dissolved pores from sample F41C2B1(figure 4.5) AFTER dissolution at magnification of 52x. Initial circular rings no longer visible instead of a net-like structure that suspects to be parts of solitary corals. Matrixes around the pores were also attacked by acid seemingly lack of any crystallized lattice structure. Zoomed in image at magnification 100x shows uniform coral features of net-like circular structure.

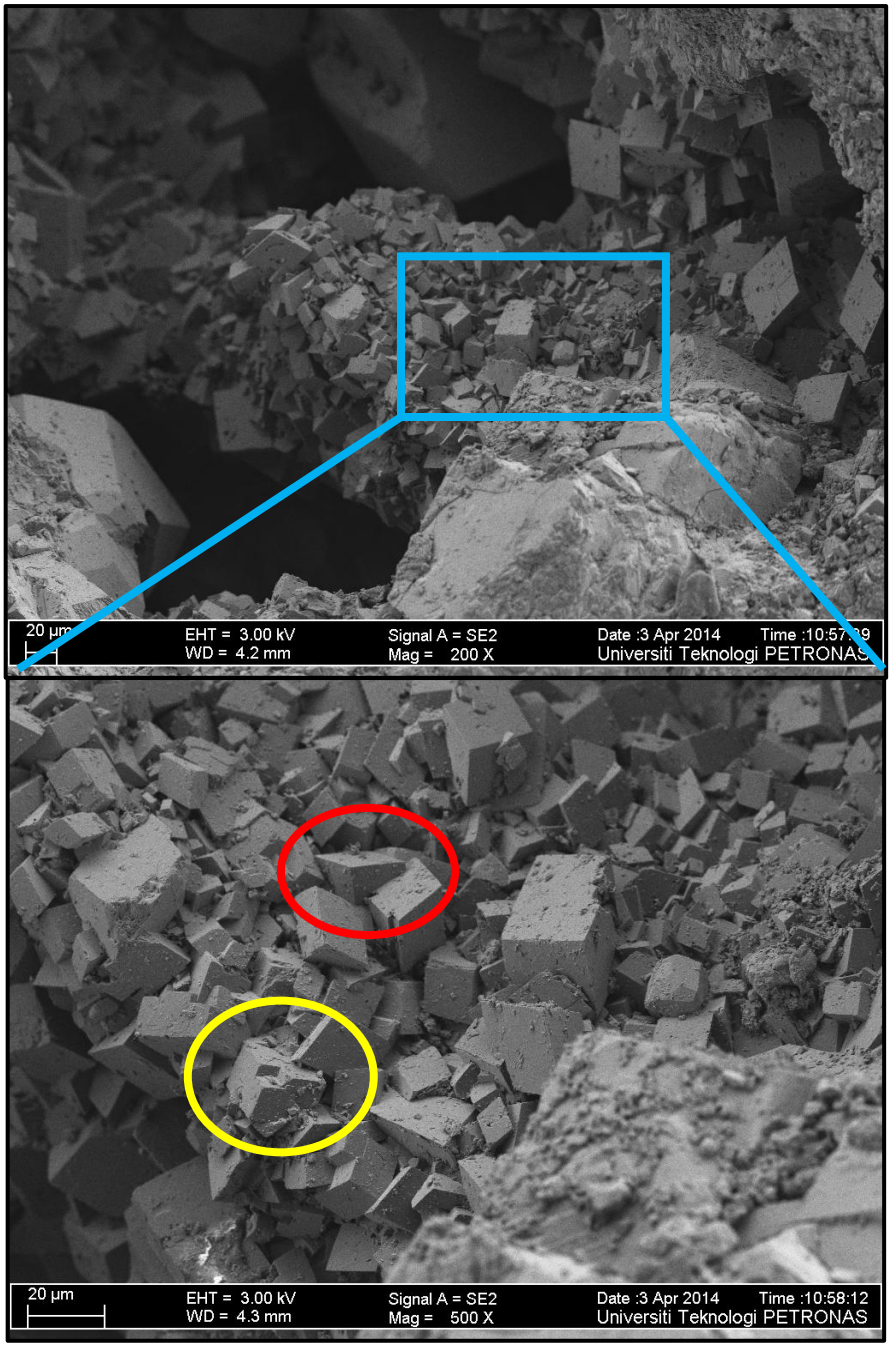

Figure 4.19: SEM images of one of the zoomed in pores at magnification of 200x from sample F41C2B1 BEFORE dissolution showing rhombohedral and euhedral crystal lattice structure that built within the pores. Obvious twinning (red circle) and imperfection of surface defects (yellow circle) were spotted from the crystals. The crystals were mostly 20-50µm in width showing several episodes of crystal development, forming medium silt size to coarse silt size.

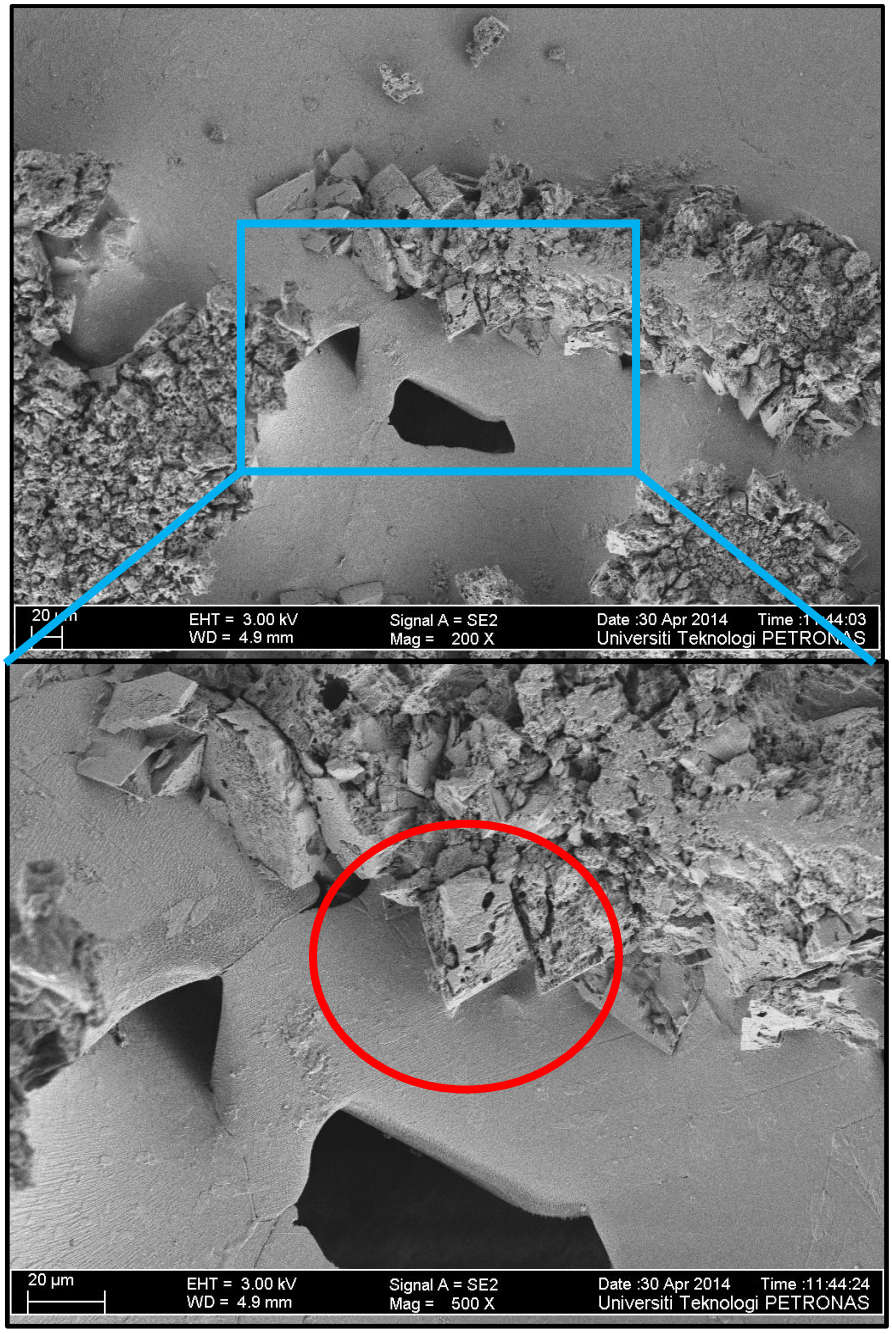

Figure 4.20: SEM images of the sample F41C2B1 AFTER dissolution showing initial pores from figure 4.7 being attacked by acid. The similar pores with lesser crystals observed and major part of the crystals were dissolved leaving a smooth surface that held the undissolved crystal. Euhedral lattice structures (red circle) were faintly recognized and surface of the crystal was covered with micro pores after the acid attack.

Facies 4A

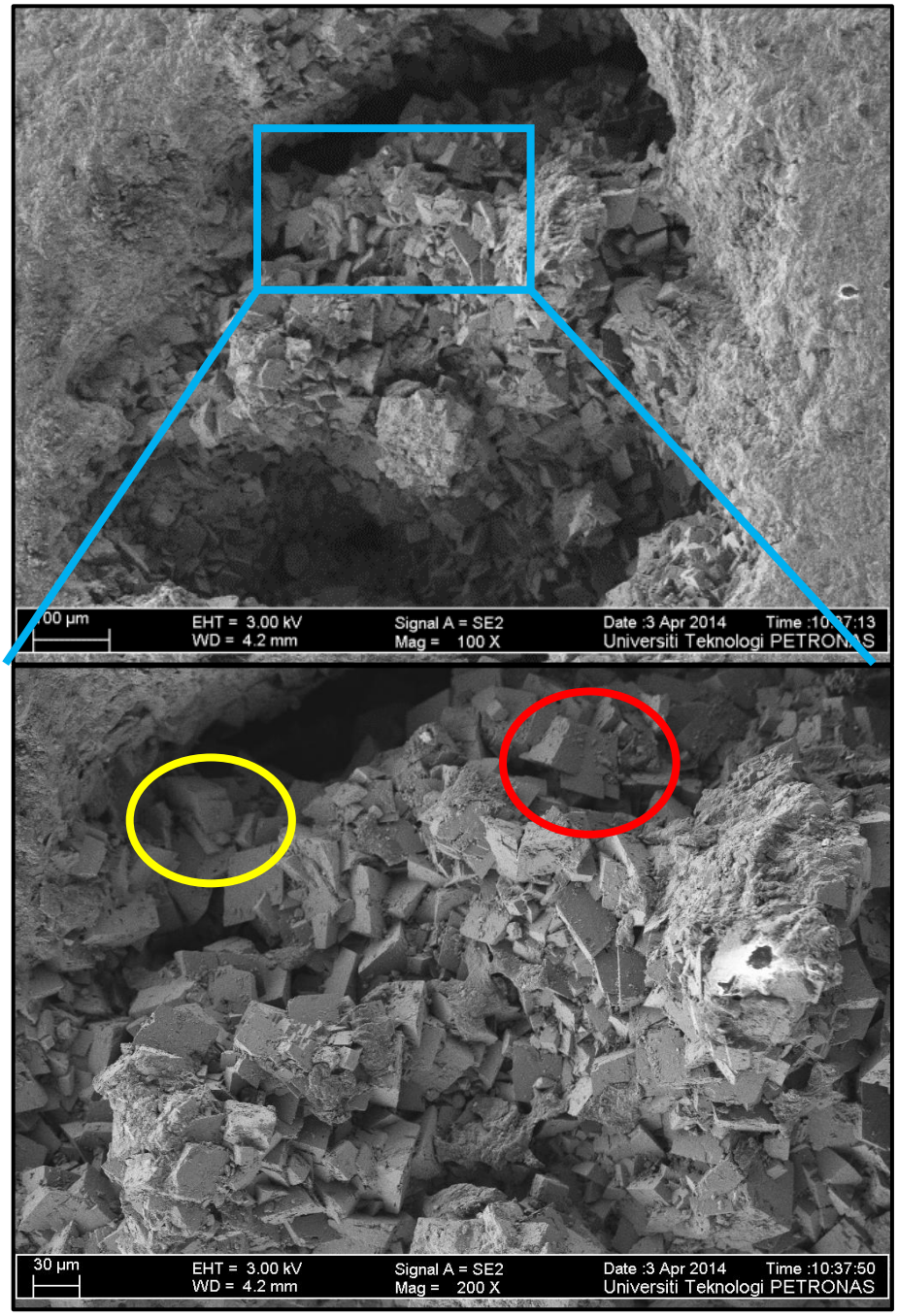

Figure 4.21: SEM images showing one of the pores of the sample F41C2B6 BEFORE dissolution at the magnification of 100x and 200x. Abundant crystal with sizes ranging from coarse silt to medium silt sizes (20µm -50 µm) were observed, displaying rhombohedral and euhedral lattice structures. Occasional twinning (red circle) and surface defects (yellow) were spotted as well.

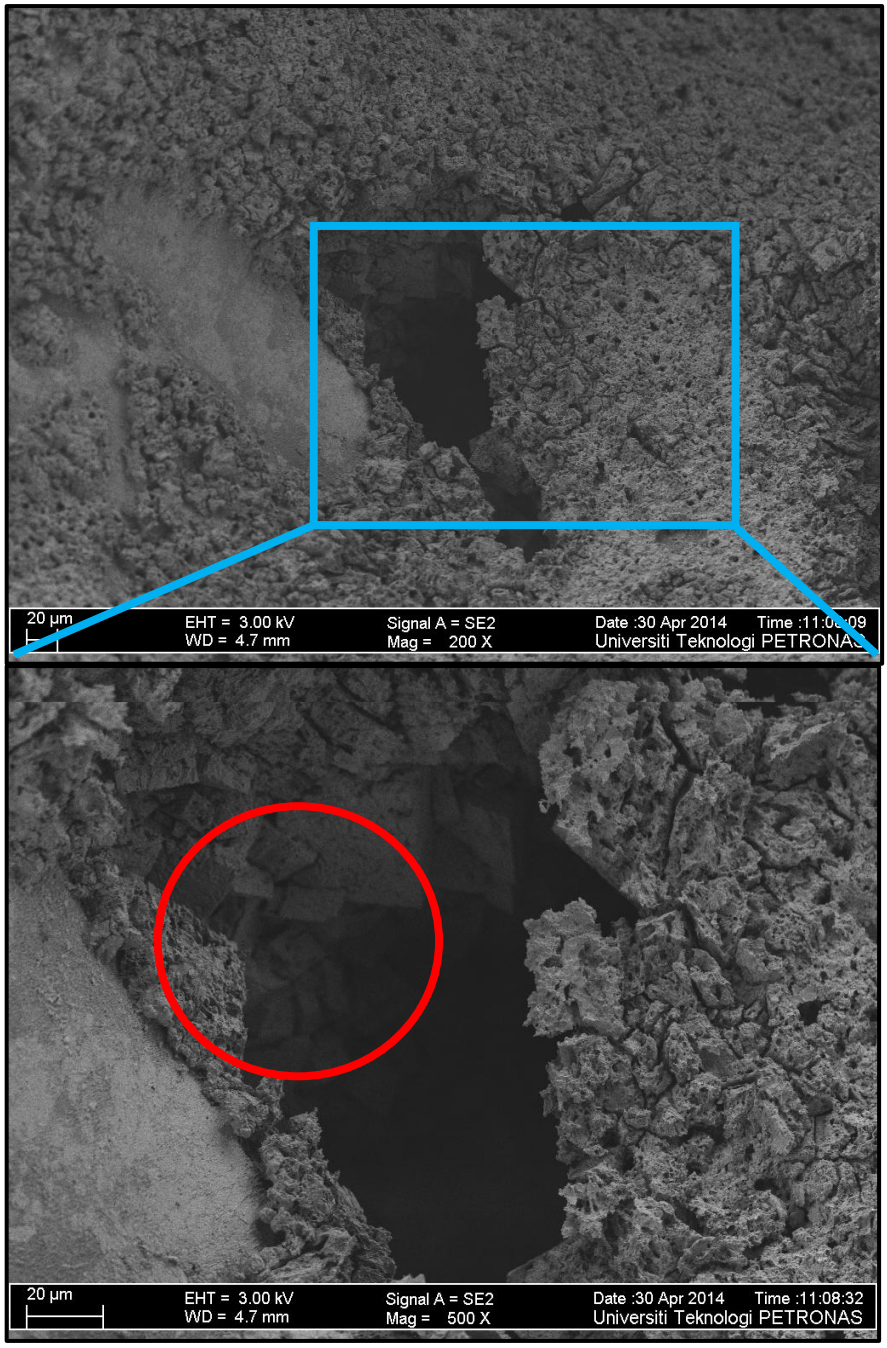

Figure 4.22: SEM images showing on of the pores of the sample F41C2B6 AFTER dissolution. Initial pore was from figure 4.9. It is observed that the surrounding surface of the pores were dissolved leaving rough surface with little notion of crystals as before. Zoomed in images at magnification of 500x showing that the inner side of the pores was less affected by the acid attack and coarse silt size rhombohedral crystal (red circle) was still visible with 20µm in width.

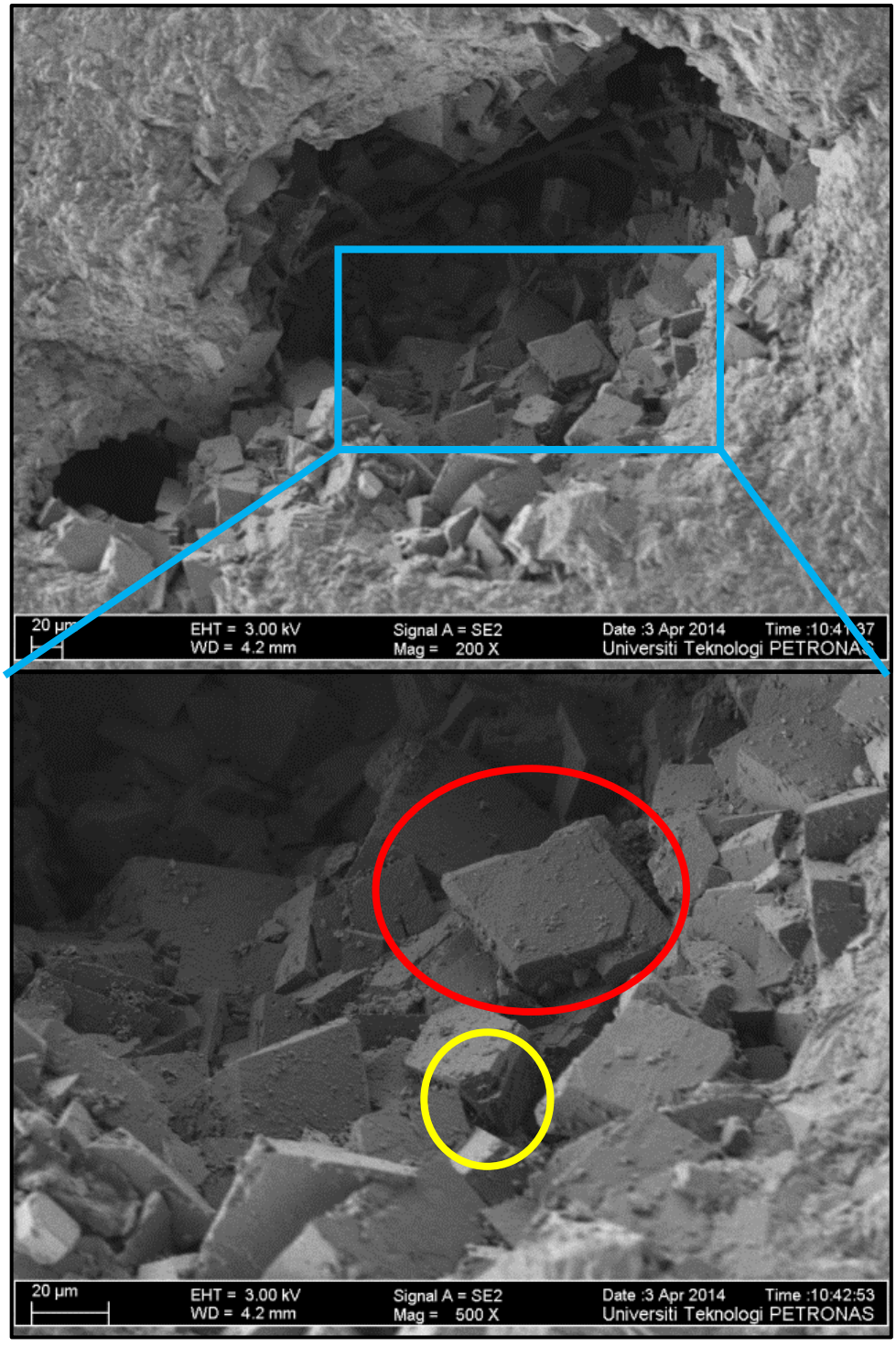

Figure 4.23: SEM images showing one of the pores from sample F41C2B6 BEFORE dissolution at the magnification of 200x. The pore was surrounded by perfect rhombohedral and euhedral crystals about 20µm-30µm in width. Twinning (red circle) and occasional surface defects (yellow circle) were observed as well within the pores.

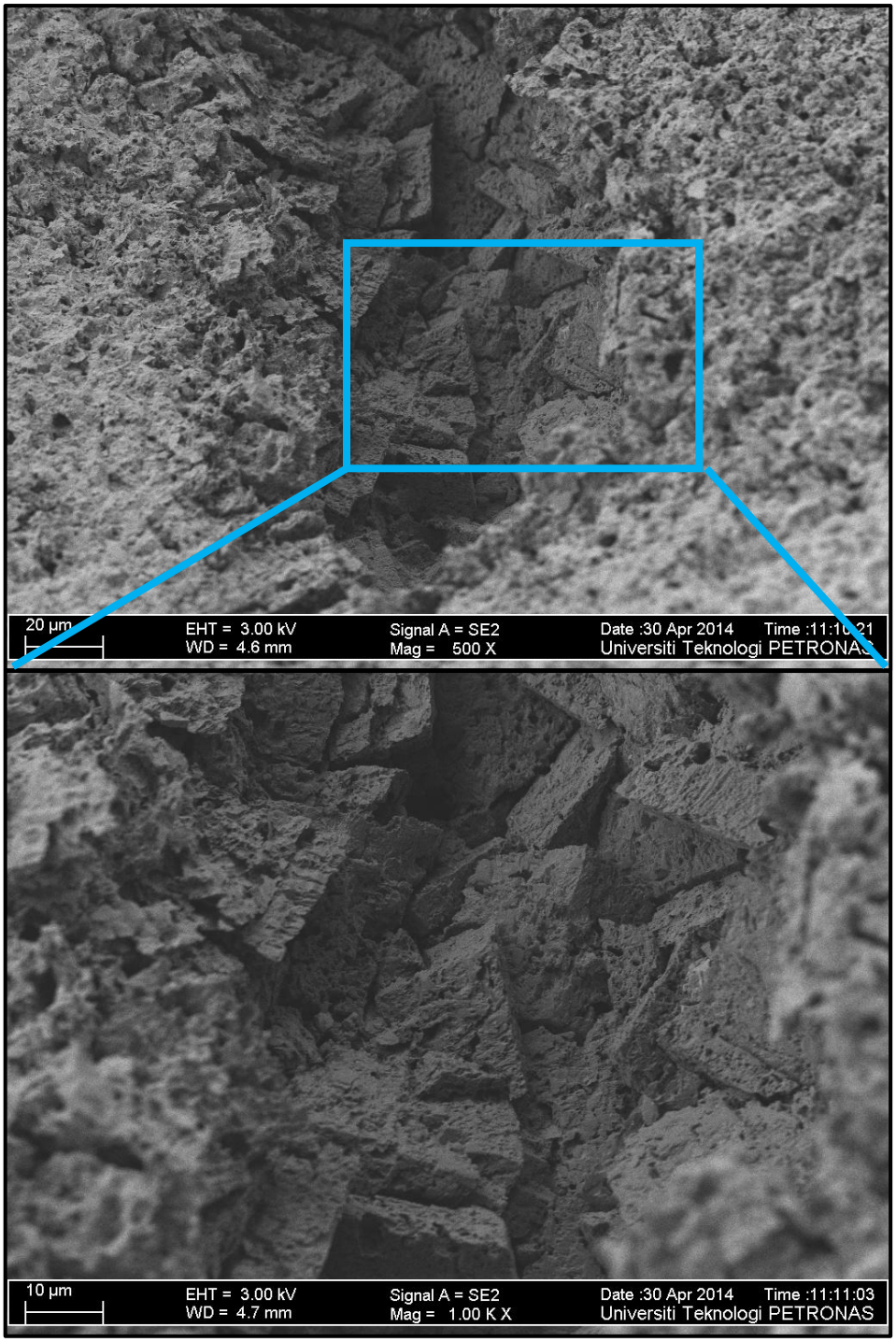

Figure 4.24: SEM images of the dissolved pore from sample F41C2B6, initial pores in figure 26, AFTER dissolution at magnification of 500x. It is observed that the crystals had prominent destructive effect after acid attack. The rhombohedral and euhedral lattice structure were destroyed and the crystals' surface has obvious micro pores about 1µm in length.

4.4 CT scan Images BEFORE dissolution

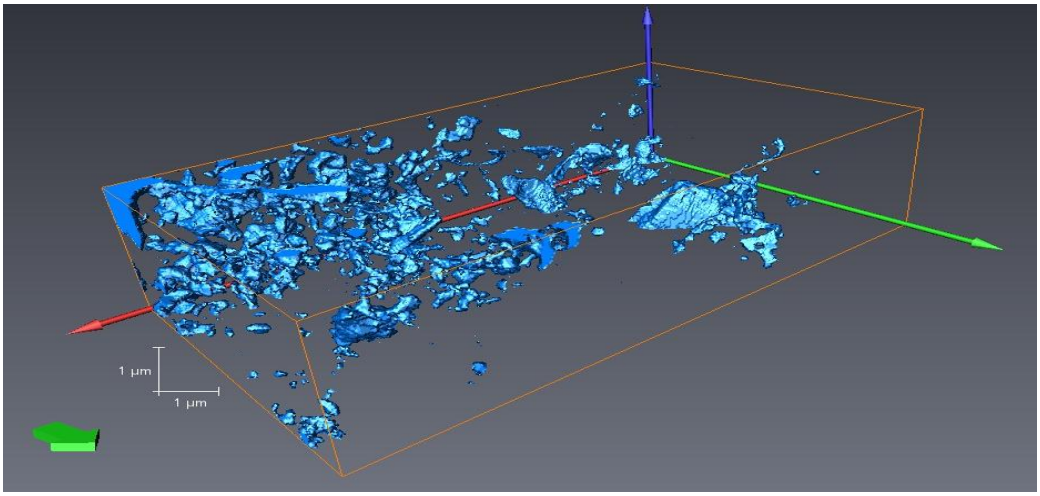

Figure 4.25: 3D pore connectivity and pore distribution of sample **F41C2B6**, from facies **4A,** with overall porosity approximately **2.73%** given the cube volume of **8mm^3**. Rendered volume of the pores showing lack of pore connectivity and non-uniform pore distribution throughout the cuboids sample.

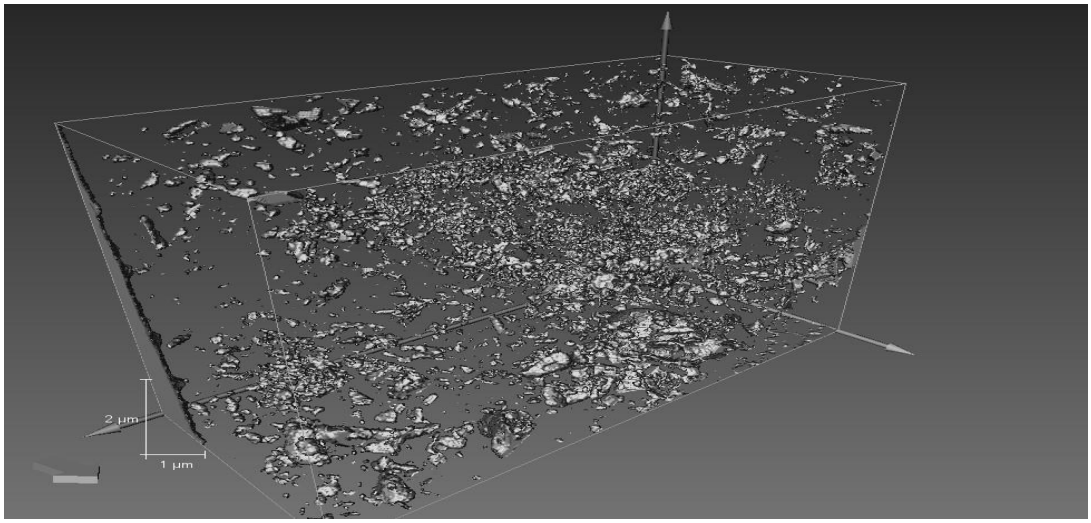

Figure 4.26: 3D pore connectivity and pore distribution of sample **F41C2B3**, from facies **4B,** with overall porosity of **3.3%** given the cube volume of **16mm^3**. Rendered volume of the pores showing more isolated pores but even pore distribution throughout the cuboids.

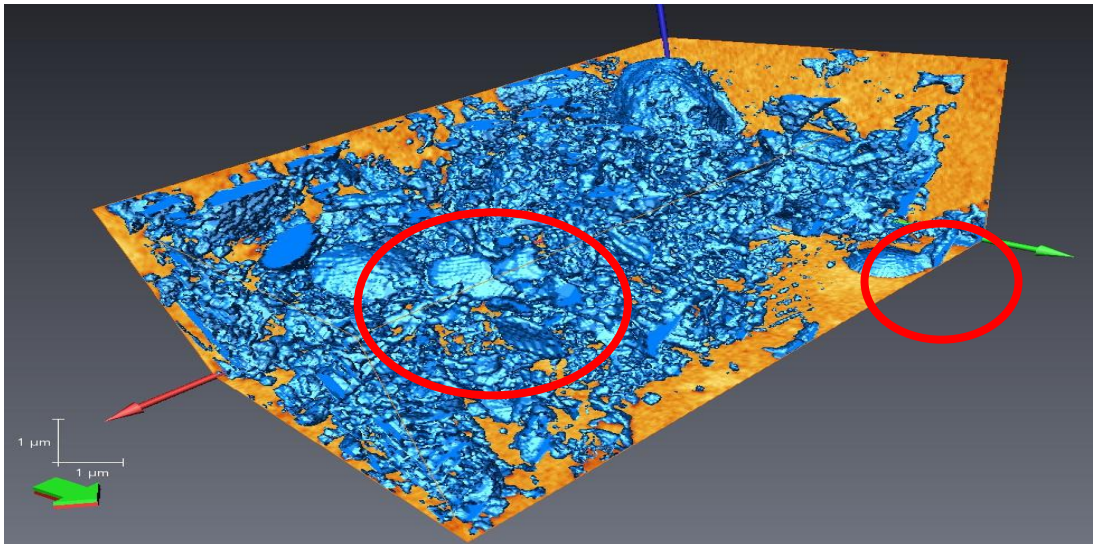

Figure 4.27: 3D pore connectivity and pore distribution of samples **F41C2B1**, from facies **4C,** with overall porosity of approximately **15%** given the cube volume of **52mm^3.** Rendered volume of the pores showing concentrated pore distribution throughout the cuboids with pores (red circles) measuring about 1mm in width, suspecting fossils or shell giving its mouldic pores.

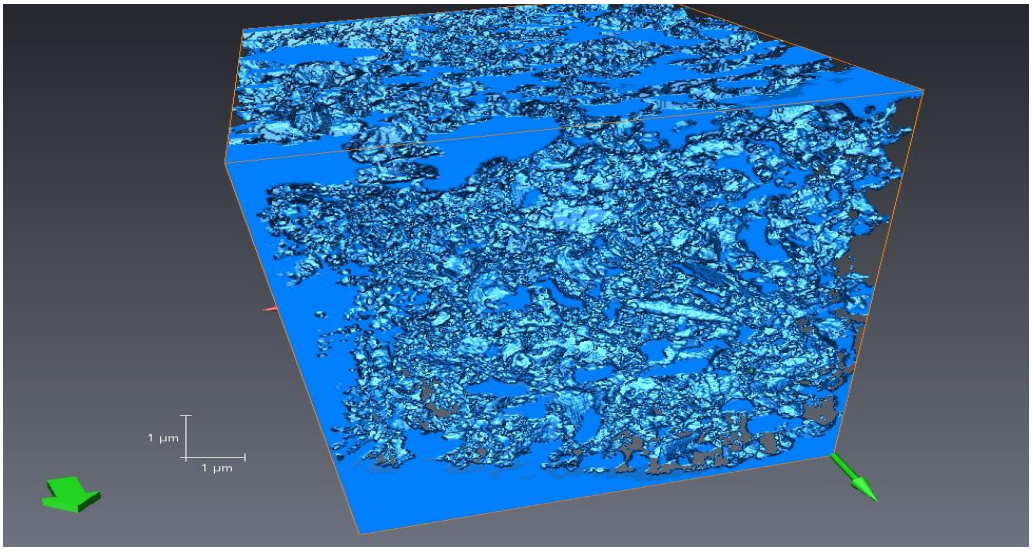

Figure 4.28: 3D pore connectivity and pore distribution of samples **F61C1B3**, from facies **6A**, with overall porosity of approximately **18%** given the cube volume of **101mm^3**. Rendered volume of the pores displaying excellent distribution and connectivity of pores throughout the cuboids.

4.5 X-ray Diffraction Analysis (XRD)

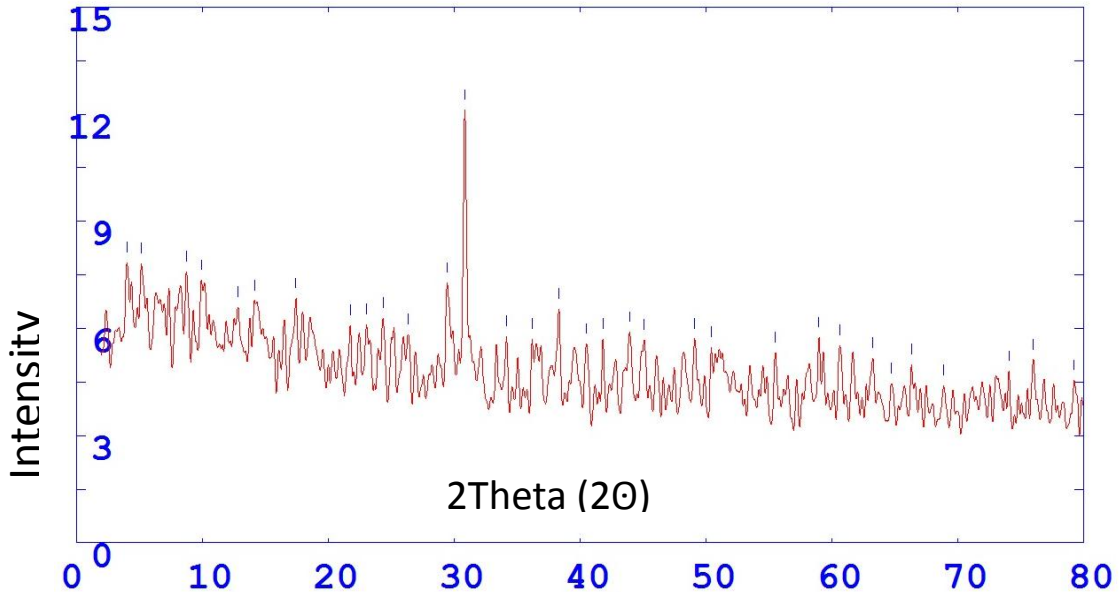

Figure 4.29: Processed XRD graph of sample **F41C2B6** from facies **4A**. Peak reading recorded having 2Θ with value 30.859 and d-spaing 2.89528 with height of 12.1, which matches with the **dolomite** standard.

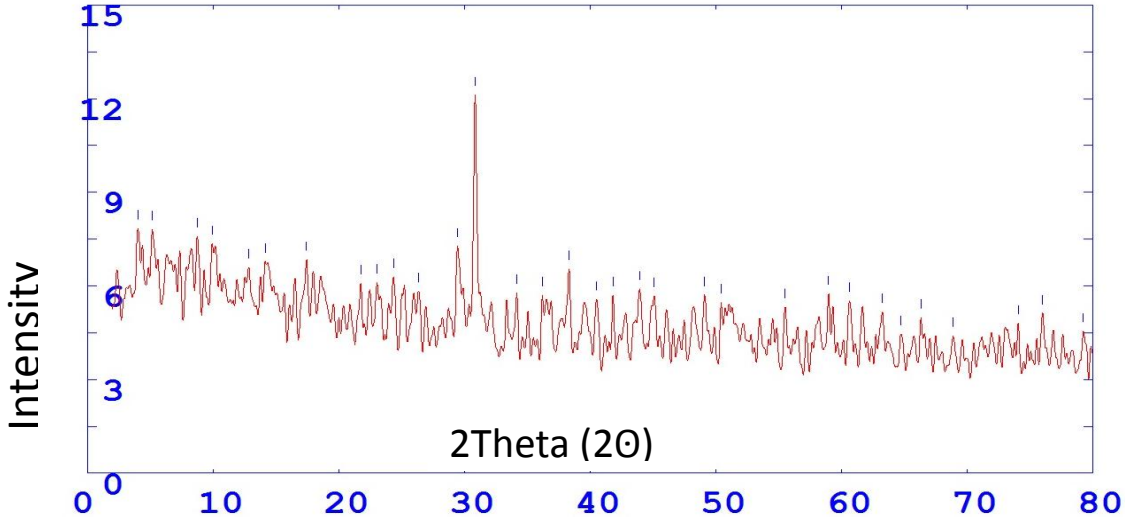

Figure 4.30: Processed XRD graph of sample **F41C2B3** from facies **4B.** Peak reading recorded having 2Θ with value 30.841 and d-spaing 2.89692 with height of 12.7, which matches with the **dolomite** standard.

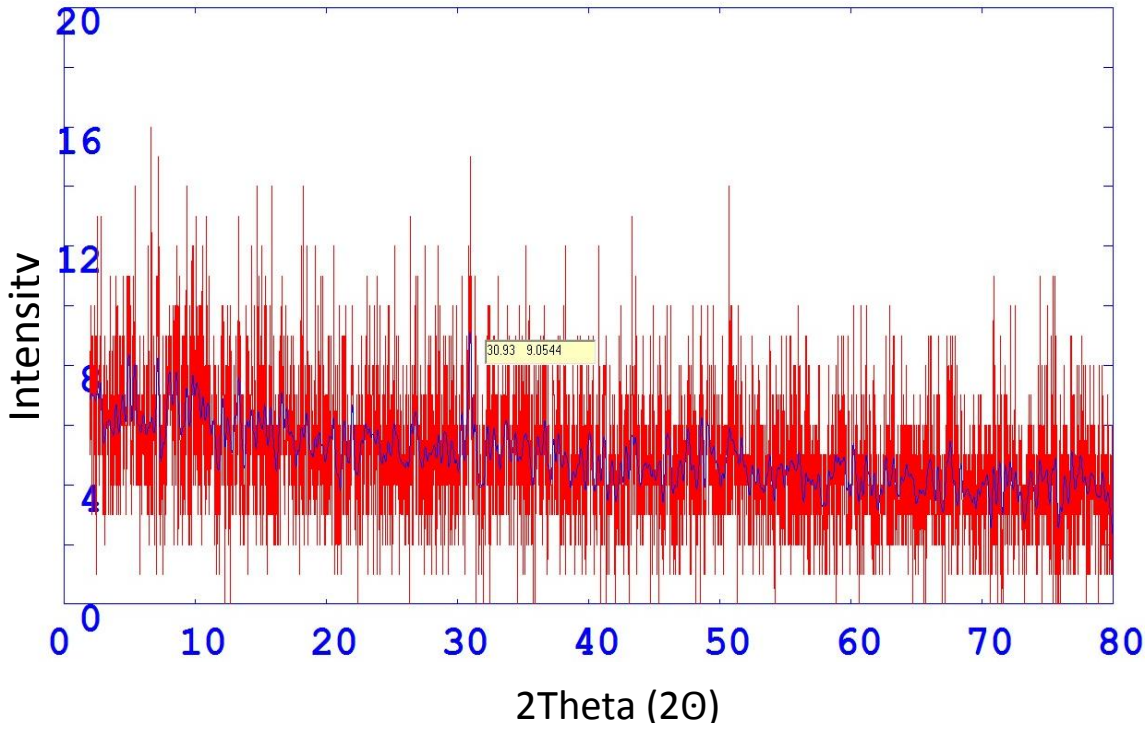

Figure 4.31: Processed XRD graph of sample **F41C2B1** from facies **4C** (blue line)**.** Peak reading recorded having 2Θ with value 30.859 and d-spaing 2.89528 with height of 12.1, which matches with the **dolomite** standard.

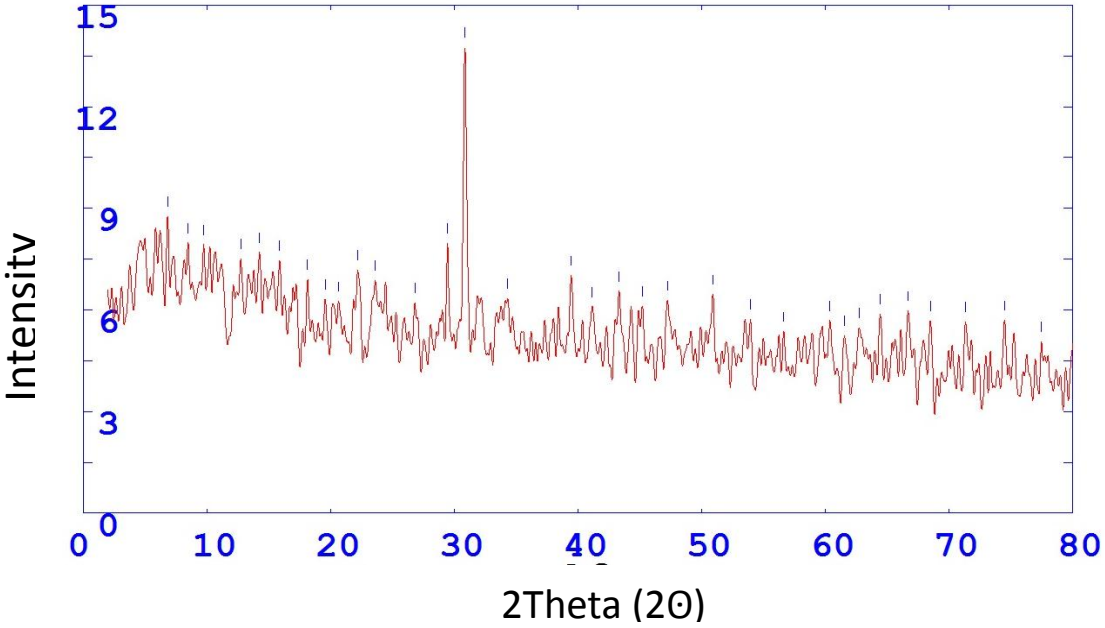

Figure 4.32: Processed XRD graph of sample **F61C1B3** from facies **6A.** Peak reading recorded having 2Θ with value 30.870 and d-spaing 2.89429 with height of 13.8, which matches with the **dolomite** standard.

4.8 Dissolution Weight Loss

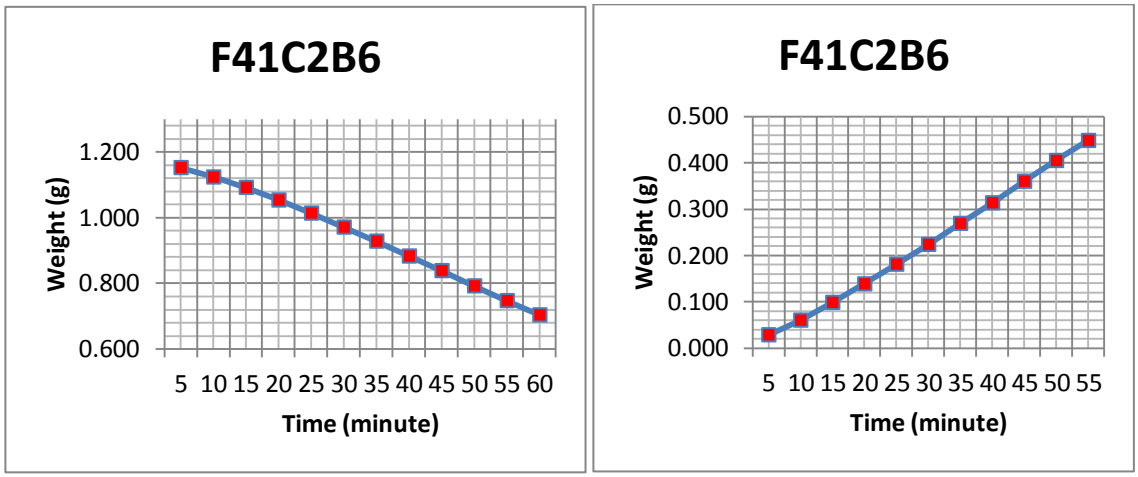

Figure 4.33: Absolute weight loss versus time graph (left) and cumulative weight loss over time graph (right) of sample **F41C2B6** from facies **4A** after dissolving in 0.01mol of HCl. Showing relatively steady trend line over time. Average rate of dissolution ranging from 0.0007g/min to 0.0057g/min.

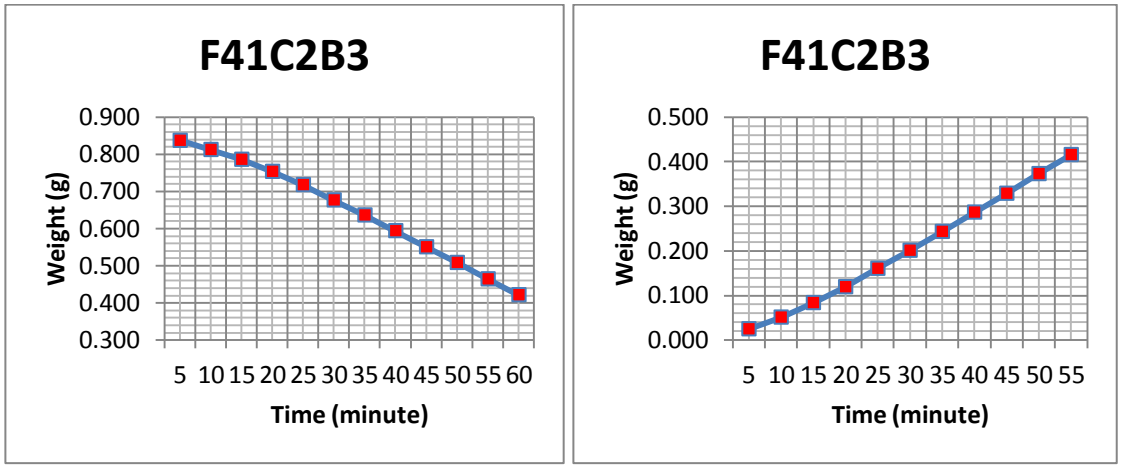

Figure 4.34: Absolute weight loss versus time graph (left) and cumulative weight loss over time graph (right) of sample **F41C2B3** from facies **4B** after dissolving in 0.01mol of HCl. Showing relatively steady trend line over time. Average rate of dissolution ranging from 0.0007g/min to 0.0049g/min.

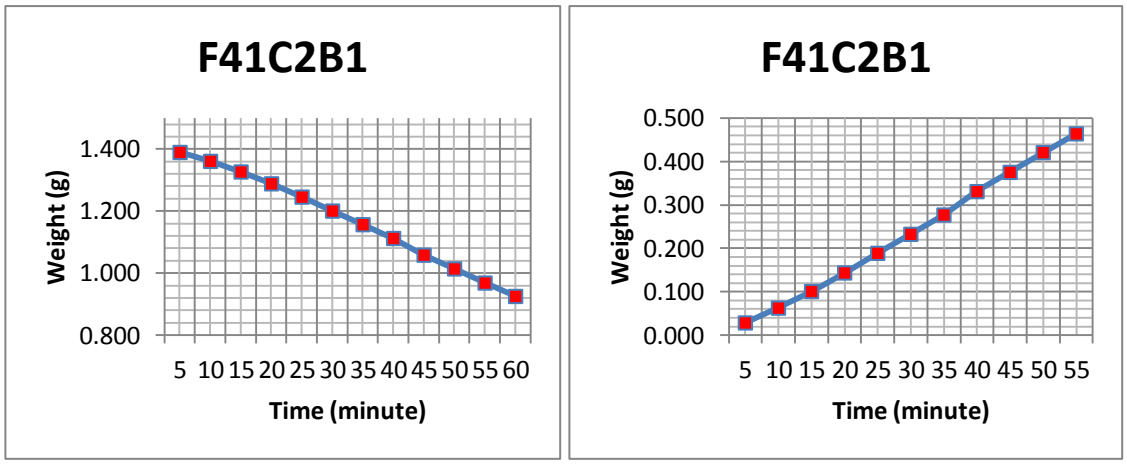

Figure 4.35: Absolute weight loss versus time graph (left) and cumulative weight loss over time graph (right) of sample **F41C2B1** from facies **4C** after dissolving in 0.01mol of HCl. Showing relatively steady trend line over time. Average rate of dissolution ranging from 0.0007g/min to 0.0058g/min.

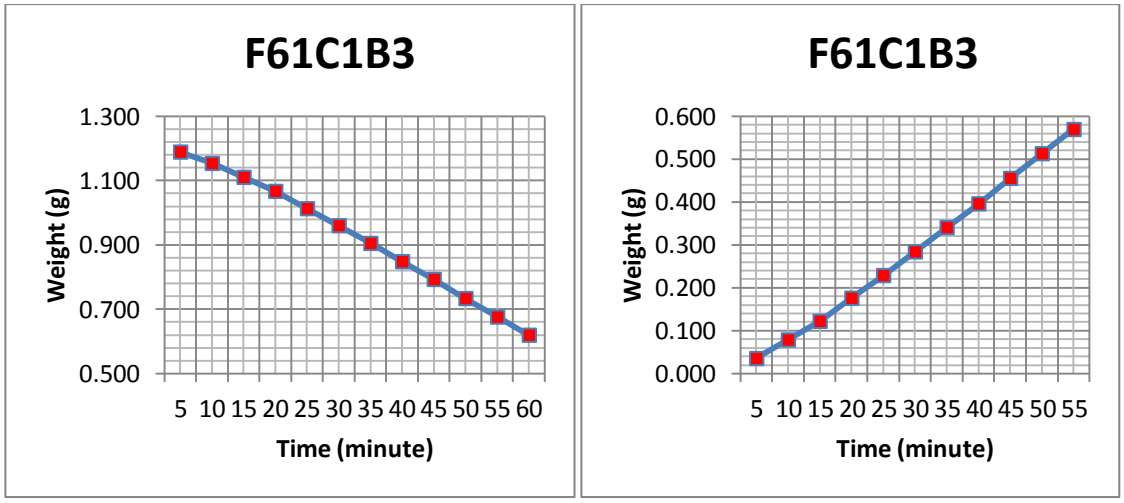

Figure 4.36: Absolute weight loss versus time graph (left) and cumulative weight loss over time graph (right) of sample **F61C1B3** from facies **6A** after dissolving in 0.01mol of HCl. Showing relatively steady trend line over time. Average rate of dissolution ranging from 0.0010g/min to 0.0071g/min.

4.6 Thermal Analysis

Table 3: Thermal data collected from the experiments.

F41C1B3 (Facies 4A)								
Q	Q/t	L	A	T1	T2	DT	k	Average k
40	0.666667	0.08	0.0066	37.5	27.4	10.1	0.80008	0.654
40	0.666667	0.08	0.0066	42.8	28.1	14.7	0.5497148	
40	0.666667	0.08	0.0066	41.9	28.7	13.2	0.6121824	
F41C2B2 (Facies 4B)								
Q	Q/t	L	A	T1	T2	DT	k	Average k
40	0.666667	0.08	0.0066	39.5	27.4	12.1	0.6678354	0.586
40	0.666667	0.08	0.0066	43.3	28.5	14.8	0.5460005	
40	0.666667	0.08	0.0066	44.1	29.3	14.8	0.5460005	
F41C2B1(Facies 4C)								
Q	Q/t	L	A	T1	T2	DT	k	Average k
40	0.666667	0.05	0.0066	35.3	26.4	8.9	0.5674725	0.450
40	0.666667	0.05	0.0066	39.7	27.7	12	0.4208754	
40	0.666667	0.05	0.0066	41.5	27.5	14	0.3607504	
F61C1B3 (Facies 6A)								
Q	Q/t	L	A	T1	T2	DT	k	Average k
40	0.666667	0.08	0.0066	34.6	23.8	10.8	0.748223	0.666
40	0.666667	0.08	0.0066	35.8	24.6	11.2	0.7215007	
40	0.666667	0.08	0.0066	40.2	24.9	15.3	0.5281574	

Tables above showed the four samples tested for thermal conductivity and the average thermal conductivity values calculated using the heat flow equation resulted in thermal conductivity (k) ranging from 0.4 to 07. Due to its low thermal conductivity values, it is interpreted that the ability of the rock to conduct heat is very low and that could be due to its low matrix contact or the lavish pore space in between matrix. Heat can be conducted easily through solid but hardly through voids. Therefore, it infers that all four samples could be possessing relatively high porosity.

4.10 Atomic Absorption Spectrometry (AAS) Analysis – Ca and Mg Concentration

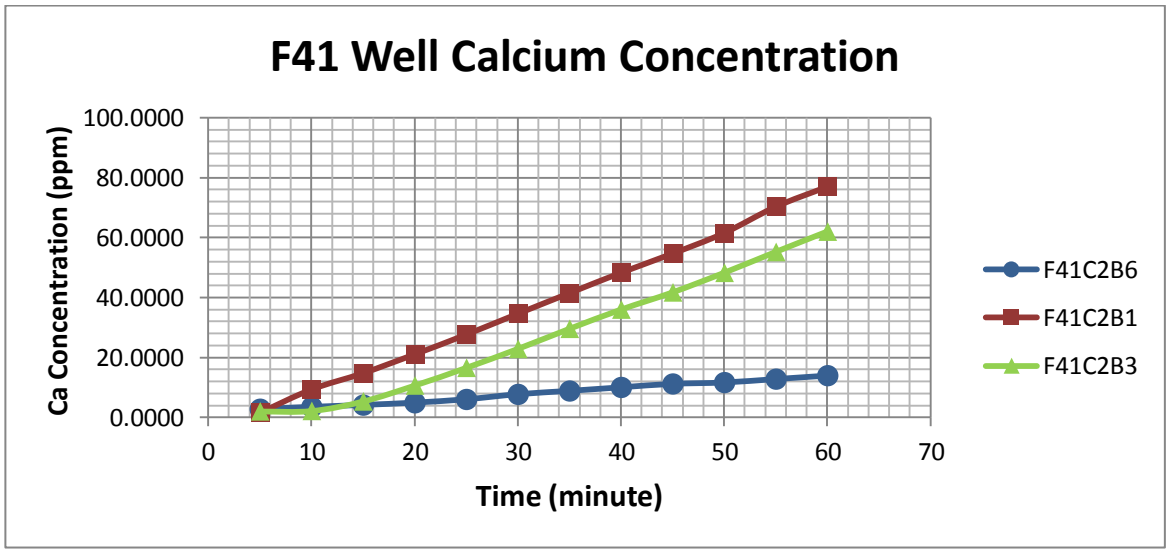

Figure 4.37: Cumulative graph of calcium concentration from three liquid samples of F41 well over 60 minutes of dissolution. Average rate of concentration ranging from 0.23ppm/min to 0.56ppm/min.

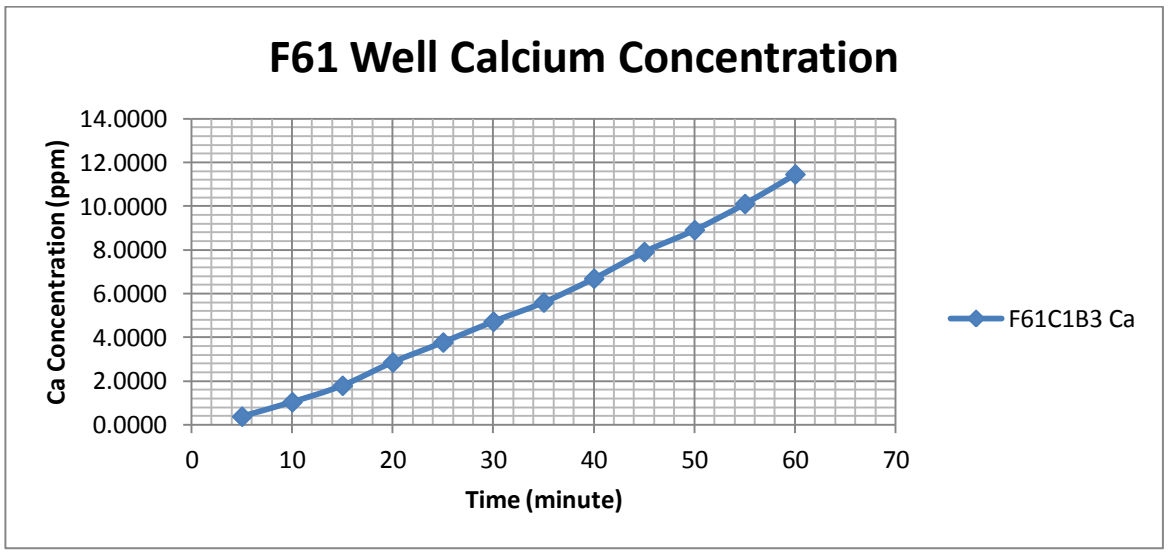

Figure 4.38: Cumulative graph of calcium concentration from one liquid sample of F61 well over 60 minutes of dissolution. Average rate of concentration ranging from 0.07ppm/min to 0.19ppm/min.

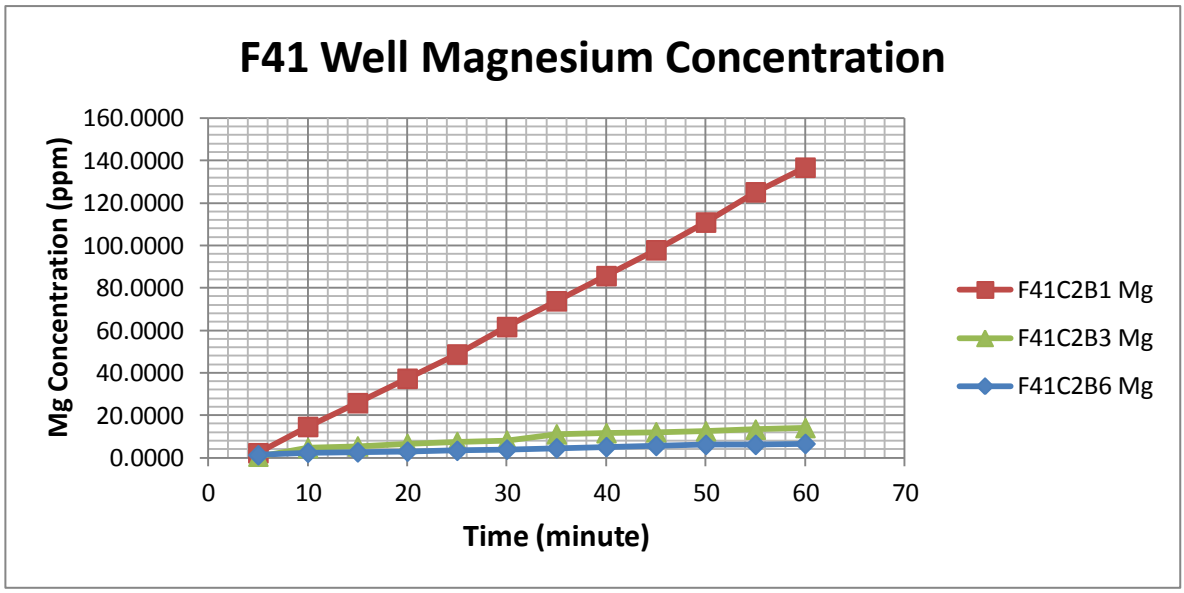

Figure 4.39: Cumulative graph of magnesium concentration from three liquid samples of F41 well over 60 minutes of dissolution. Average rate of concentration ranging from 0.11ppm/min to 0.25ppm/min.

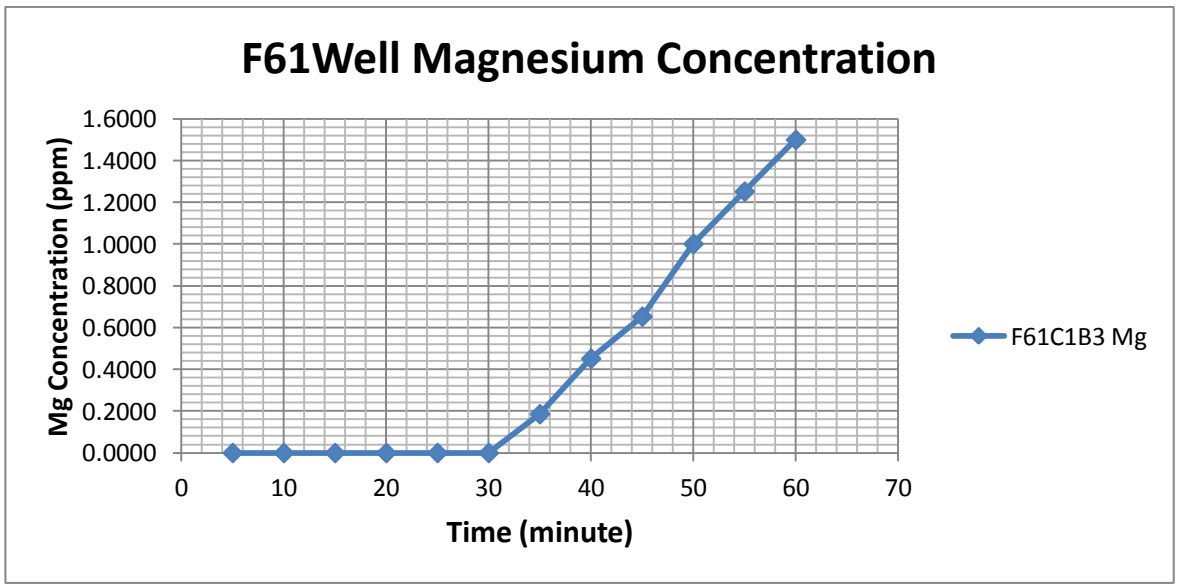

Figure 4.40: Cumulative graph of magnesium concentration from one liquid sample of F61 well over 60 minutes of dissolution. Average rate of concentration ranging from 0.005ppm/min to 0.025ppm/min.

4.11 Analogue Mapping

Figure 4.41: Aerial map of Hill A, before part of the limestone hill was quarried.

The research outcrop was situated at the position of N 04 51.496, E 101 07.309 and located just in the middle of oil palm plantation, covering an area of about 1000m x 400m. The targeted outcrop was actually a limestone quarry and referring to initial aerial view (figure 4.25) of the outcrop, 30% of the hill has already been quarried. Therefore, lithology boundary between the limestone hill and the surrounding lithology was faintly identified by dotted line at the west and east side of the outcrop. This was due to the quarries pushover that might have blurred the boundary of lithological contact with the surrounding lithology, the true boundary at the two sides of the hills was certain from

the current outcrop. However, after thorough traversing around the limestone hill, the contact at the north and south side of the hill were found and confirmed. Both sides of the hill were having a sharp contact with surrounding reddish and brownish sediments that was typical of limestone precipitation of magnesium. It has been certain because of the observation of high escarpment at the north side of the hill but right next to it has no evidence of limestone remnant, only vegetation at lower ground. For the south side, traversing is yet to be conducted due to limited accessibility, but overlooking from the top of the outcrop, the contact was certain as the southern part across the outcrop has a smaller limestone hill that was suspected to be the similar stretch of the outcrop situated about 500m away. The sharp contact next to it was also similar with that at the northern side – high escarpment and vegetation at lower ground right next to it. Thus, albeit the pushover at the western and eastern side of the outcrop, overall, it is interpreted that the surrounding lithology was the reddish and brownish sediments which has now been covered by oil palm plantation.

In this study, only the major limestone hill (Hill A) was studied. In terms of facies, there were total of 6 facies encountered through multiple traversing and observations, each time scrutinizing more facies in details. From the most southern part of Hill A, the facies observed was typical limestone characteristics, light to dark grey in color and having crystals about 2mm in size under hand lens observation. Thickness of this facies was about 30m from ground and about 30m wide, having 3-5 major fractures dipping inwards the rock units. This unit was then classified as *light to dark grey crystallized limestone*. Gradually after the light to dark grey crystallized limestone, another similar facies was encountered but with darker grey in color. It is interpreted that the darker grey was contributed by the dolomitic nature of the rock, and it possessed similar crystals, slightly larger size, about 3mm, with the previous rock unit. The massive units had no visible fractures running across the bed. Thus, the facies in this unit was classified as *dark grey crystallized limestone*. Moving up to the north-west direction of the hill, the facies gradually changed into light grey limestone complemented by spots of dark grey dolomitic elements within the matrix. The formation of this facies was understood after one of the boulders was seen to have obvious secondary reprecipitation

of calcium carbonate within the dolomitic matrix. It was interpreted that the calcitic part of the rock was actually secondary reprecipitation of carbonate deposits between the pores of the dark grey limestone, thus cementing the loose matrix of dark grey limestone with the recrystallization of calcite. It was evidently accurate with the discovery of a few caverns found at several points of the hill and also the formation of stalactites and stalagmites. This could explain the intrusion of meteoric water that dissolved the carbonates and then precipitated into other parts of the hill through fractures or cracks.

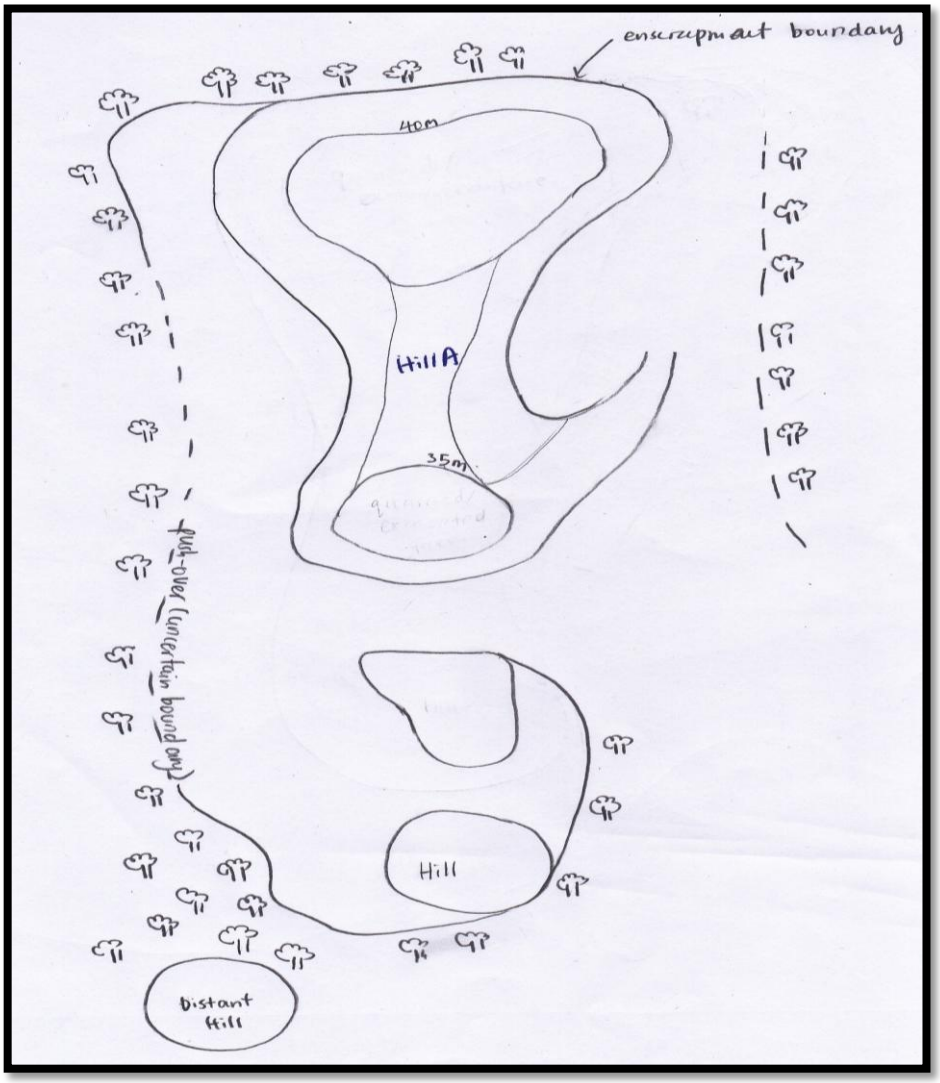

Figure 4.42: Plan view sketch of the quarries in current day, showing undefined litholgy boundary (dotted line) and defined lithology boundary (solid line) of the hills.

This unit was then classified as the *light grey calcitic limestone with spotted dark grey dolomitic matrix*. At the north-eastern side of the hill, however, the facies encountered were barely intact to the hill. It was observed that the facies here were heavily fractured with joints millimeters in length, especially at the surface of the unit. This facies stretches about 50-100m wide across the eastern side to the back of the hill and about 60m in thinkness. The unit was first interpreted as heavily jointed facies with perhaps different rheology with the neighbouring facies, however, detailed scrutiny (fresh rock yet to expose to physical weathering) brought to enlightenment that the rocks were banded with alternating calcite and dolomite lamination, each banding about 2cm. It was then interpreted that the heavily jointed surface might be due to the weak plane of the bandings, especially at the contact of lamination. Thus, this unit was classified as the *banded and heavily fractured limestone.*

At the top of the hill, nearer to the northern part, two types of facies were found. One at the top western part was classified as *dark grey dolomite with white calcitic veins* whereas the facies at the top eastern part were classified as *whitish crystallized limestone*. A sharp contact of these two facies was found, inferring abrupt changes of facies and hence delineating the facies boundary between these two facies. The dark grey dolomite was found with massive calcite invasion at all parts of the rocks and also 5-6 similar sets of fractures running across them, suggesting the invasion of calcitic veins within the dolomite. It was interpreted that the carbonates behaved similarly with the spotted limestone at the bottom, similarly at the western part, of the hill, whereby the joints or cracks were infill exactly like the reprecipitation or recrystallization of calcite due to dissolution and intrusion of meteoric water observed from the spotted limestone. A cave (similarly the cavern features –stalagmite and stalactite) was found too at the tip of the hill, thus evidently strong suggestion that the difference of facies from top to bottom, albeit at the same segment of the hill, was due to secondary deposition of carbonates between any possible pores and cracks throughout the unit because of meteoric water intrusion. Both the top and bottom western side of the hill were similarly having dark grey limestone of matrix but were then invaded by secondary deposits within voids (the bottom facies) and cracks (the top facies). The top eastern side of whitish crystallized

limestone was however, lightly jointed, similar with the bottom eastern part of banded and heavily jointed limestone. This had suggested that the eastern segment of the hill was probably made up of slightly similar rock, having the almost similar rheology.

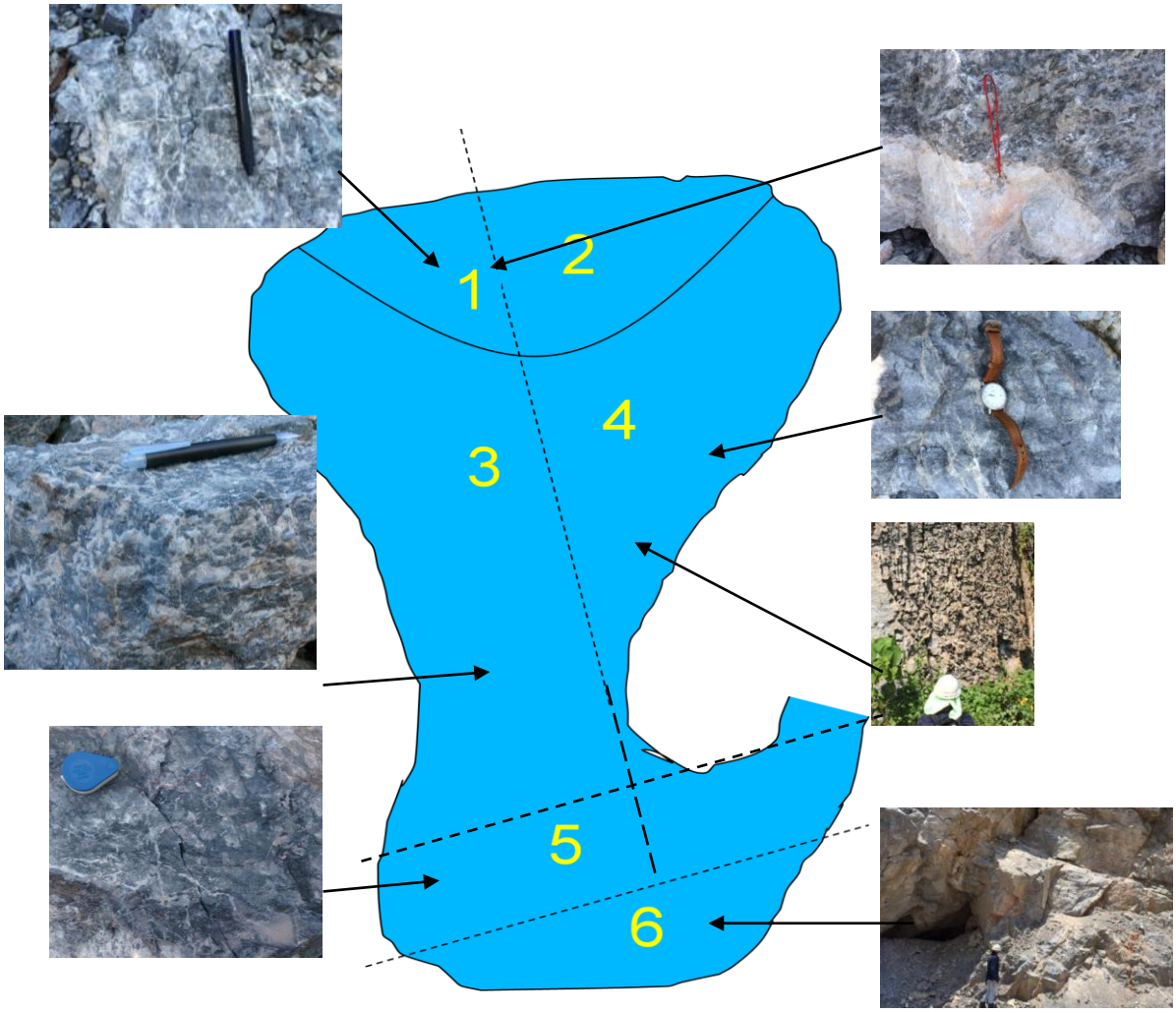

Figure 4.43: Plan view sketch of Hill A showing pre-determined facies boundaries and facies types. (Top left clockwise) Dark grey dolomite with white calcitic veins, contact between dark grey dolomite and whitish crystallized limestone, banded limestone, heavily fractured limestone, light to dark grey crystallized limestone, dark grey crystallized limestone and light grey calcitic limestone with spotted dark grey dolomitic matrix.

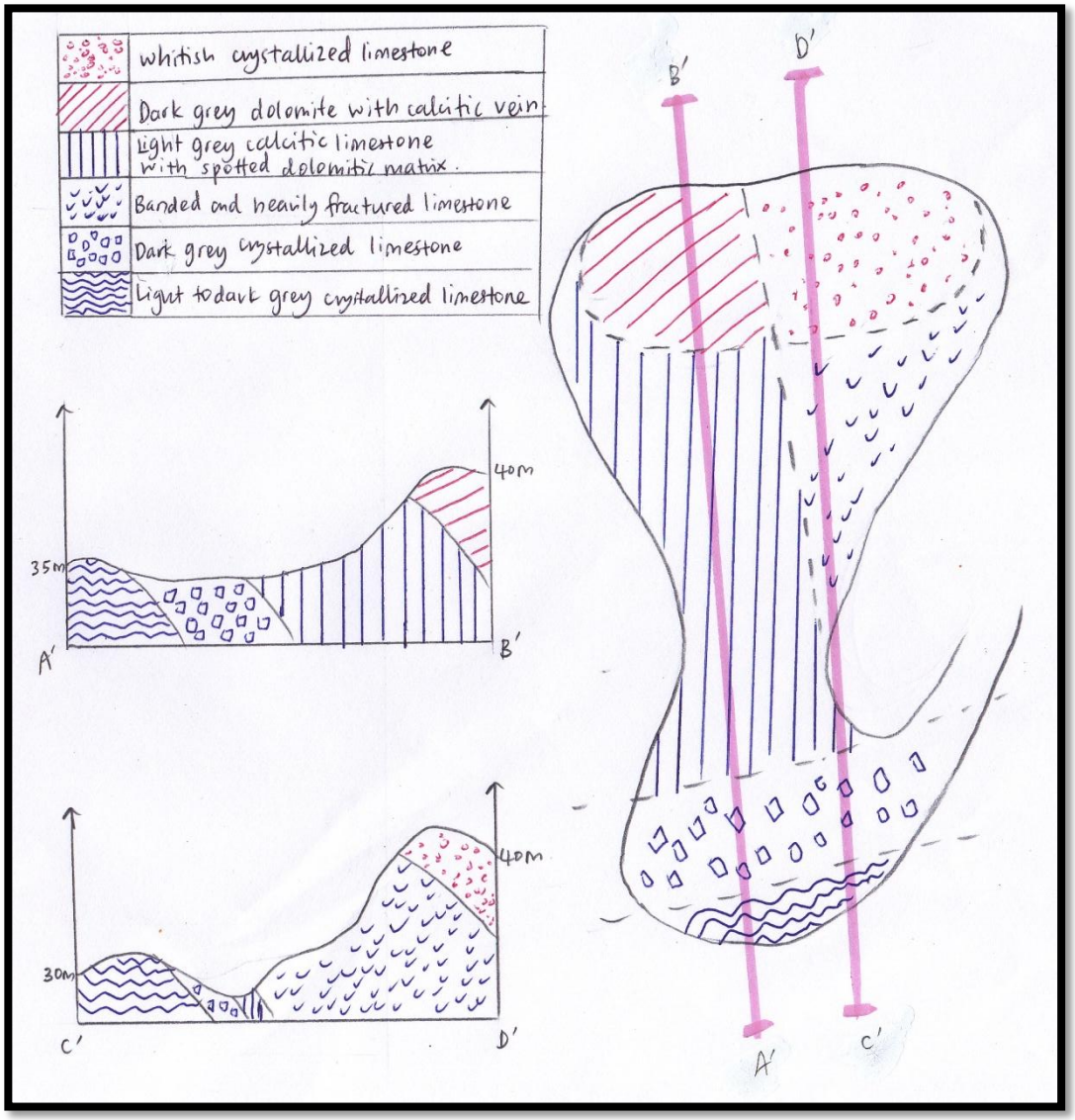

Figure 4.44: Sketches of Hill A with pre-determined facies boundaries and cross-sectional view of the eastern and western segments of the hill.

The facies boundaries had been faintly derived from the encountered facies along the traversing path. With the joints, fractures, and possible bedding measurements, the cross section of the Hill A was as shown in figure 4.28, showing both segments of the hill. Generally, from the cross section, it is shown that Hill A had an increment in elevation from the south to north and facies changes across the facies boundary dipping at an angle of approximately 30°. Further investigation of the rock units, in terms of spatial distribution, the outcrop here had almost near zero porosity, at least to the naked

eye observation. No visible pores were encountered even under the hand lens. This has evidently suggested that, the primary pores might have already been infill by secondary mineral after several episodes of diagenetic events. Thus, principally, no traces of fossils were encountered due to the preservation condition of the rock units were not favorable.

In its entirety, the analogue limestone hill in Sungai Siput has served to be a comparative model in this study. However, after all the investigations and scrutinizes of the facies from both offshore cores and onshore outcrop, there were no any correlatable facies between the samples. Theoretically, the Sungai Siput outcrop was at the period of Ordovician to Silurian whereas the carbonate buildups in Central Luconia were from Middle Miocene. The main reason to comprehend the lack of similarity of the two carbonate formation was the age and also the climate differences during the times. As per understood, carbonates buildups are sensitive to several climatic factors like temperature, acidity, pH and etc. All these factors are built on the difference in partial pressure of CO_2 in air and water. In theory, carbon dioxide dissolves in the ocean to form carbonic acid (H_2CO_3), bicarbonate (HCO_3^-) and carbonate (CO_3^{2-}), and there is already about fifty times as much carbon dissolved in the sea water of the oceans as exists in the atmosphere.

During the Upper Ordovician, a major glaciation centered in Africa occurred resulting in a severe drop in sea level which drained nearly all carbonate platforms. This glaciation had contributed to ecological disruption and mass extinctions during the time due to abrupt changes of climate. Gradually coming into the period of upper Silurian, a deglaciation and rise in sea levels had then created many new marine habitats, providing the framework for significant biological events in the evolution of life. Coral reefs, made their first appearance in the fossil record during this time. Shallow clear waters during Ordovician over continental shelves encouraged the growth of organisms that deposit calcium carbonates in their shells and hard parts, providing evidences of favorable climate for carbonate formation during that period of time. Whereas during the Middle Miocene, Earth's climate transitioned from a relatively warm phase (Miocene climatic optimum) to a colder mode with reestablishment of permanent ice sheets on Antarctica,

thus marking a fundamental step in Cenozoic cooling. Carbon sequestration and atmospheric CO_2 drawdown through increased terrestrial and/or marine productivity have been proposed as the main drivers of this fundamental transition. Hence, this has shown that, the principal difference in Sungai Siput outcrop and Central Luconia buildups were due to the difference in paleaoclimate that closely related to the paleo depositional environment, favoring different deposits of carbonate.

Albeit the Hill has now gone through several episodes of diagenetic event and now dominant by secondary deposits, the occurrence of the limestone formation were still similar of that to the Central Luconia Buildups, where both of carbonate units were formed at the optimum carbonate production condition. The only difference was the degree of exposure of the rock units to diagenetic events. This can be easily explained with the spatial distribution of the rock units and fossil contents. Apparently the Sungai Siput limestone hills with near zero porosity and absence of fossils had exposed more to diagenetic events compared to that from Central Luconia, having relatively high porosity reaching the figure of 17% and also multiple fossils discoveries from petrography analysis. The Sungai Siput limestone hill might initially have porosity similar to those of Central Luconia, perhaps due to the long term exposure to diagnetic events, the secondary deposits had recrystallized and infill the pores, left it with zero porosity. In fact, the Central Luconia buildups are experiencing secondary mineral infill too as shown in the SEM images (figure 4.13 – 4.20). Medium to coarse silt size of crystal were evidence of recrystallization starting to build up within the pores. Future envision of the pores in Central Luconia buildups could be similar to the Sungai Siput outcrops? On the other hand, in terms of fractures and joints, both carbonate units are depicting rather contrasting features. Sungai Siput outcrops has joints and fractures that ranges from centimeter to meter but the Central Luconia cores are having fractures associated with pressures and tensile stresses, where stylolite features were visible within the vertical cores and the next stylolite within the core would be 5meter away from the previous one. This difference of fracture's features could be due to the difference of rock rheology and thus the carbonate composition. Externally, it could be due to the degree of physical weathering of the carbonate units. Back to the explanation of meteoric water

intrusion and cavern formation, it is evidently strong to suggest that the Sungai Siput outcrop had higher degree of exposure to physical weathering and hence, forming joints with centimeter in length as compared to the meters in length stylolite found in the Central Luconia cores. The stylolite features is an indication of tensile stresses acting upon the rocks, possibly due to the overburden pressure.

From the gathered results and data, it is interpreted that the F41 well is having 3 distinctive facies identified according to core logging and it is supported by its difference of porosity and permeability throughout the log. The CT scan images too, showing three distinctive distributions of the pores throughout the cubes. Therefore, the well F41 can be easily distinguished by its pore network differences. However, in terms of mineralogy, all three facies are having comparatively similar elements and mineral from the EDX and XRD results. Evidently, even having distinctively unalike porosity and spatial distribution, it is still possible to have similar elements and mineral forming the rocks. That is because with the same minerals, there are still many possible ways of connecting them in terms of structures. Rhombohedron structure is the ideal state of stability for calcite, however, if there exists twinning and surface defects as shown in the SEM images, it is conclusive that the binding of the crystals are weak. This is because twinning crystals are sharing ono side of their structures, the binding points of the structures is the weak points and can be easily attacked by other elements. The SEM images captured the crystal structure from facies 4A showing the best example of crystal twinning, and proving it to be weak bond with the AAS results that have the highest concentration of calcium after dissolution, albeit the steady rate of dissolution. The reason of having high concentration of calcium could possibly because of the acid attack to the weak bonds that bind the crystal together. Once the acid being attacked, the crystals could be shredded into the acid solution thus recording high concentration of calcium.

CHAPTER 5

CONCLUSION & RECOMMENDATION

Carbonates are prone to diagenetic dissolution in terms of pore network and spatial distribution, this holds true in both F61 and F41 wells evaluated in this study, and becomes more evident during quantitative evaluation of porosity at multiple scales of observation. With all the gathered information from all the analyses, it is shown that the objective to study the impact of dissolution diagenesis on carbonate pore network is achieved. The difference in rock fabric, which was contributed by the different depositional environment and alos post diagenetic events, did played an important role and contributing factors in the difference of dissolution and thus, pore network in the carbonate of F-field Central Luconia. The understanding of pore behavior has been understood from the rate of dissolution curves and also from the post dissolution SEM images. It has been confirmed that prolong exposure to acid, which equivalent to dissolution diagenesis on carbonate rock has significant impact on the pore network. It enlarges the pores and thus contributing to better pore connectivity. However, the degree of pore changes still largely depending on the facies type as well as the mineral composition of the rock unit. Better understanding of the pore behavior in the F-field well could be employed in future work of EOR and also further reservoir characterization.

On top of which, The understanding of the carbonate difference were achieved by studying the analogue limestone hill of Sungai Siput, Perak as well as detail studies and core analysis on two F-field wells. The analogue model has served its purpose of a standard comparative model to understand the likely depositional environment and envisioned diagenetic events between the onshore outcrop and the offshore sample.

REFERENCES

(2012, March 1). Retrieved July 7, 2014, from Ipoh Echo: http://www.ipohecho.com.my/v2/2012/03/01/kinta-valleys-limestone-hills-and-caves/

Ali, M. Y., & Abolins, P. (1999). Central Luconia Province. In *The Petroleum Geology and Resources of Malaysia* (pp. 369-392). Petroliam Nasional Berhad (PETRONAS).

Anderson. J.A.R. & Muller, J. (1975). Holocene peat and a Miocene coal deposit from NW Borneo. *Rev. Paleobot.Palynol,* , 19, 291-351.

Boever, E. D., Varloteaux, C., Nader, F., Foubert, A., Békri, S., Youssef, S., et al. (2012). Quantification and Prediction of the 3D Pore Network Evolution in Carbonate Reservoir Rocks. *IFP Energies nouvelles* .

Choquette, P. W., & Pray, L. C. (1970). Geological Nomenclature and Classification of Porosity in Sedimentary Carbonates. *AAPG Bulletin* , 207-250.

Dong, H., Fjeldstad, S., Alberts, L., Roth, S., Bakke, S., & Øren, P.-E. (November 2008). Pore network modelling on carbonate: a comparative study of different micro-CT network extraction methods.

Epting, M., "Miocene carbonate build ups of Central Luconia, offshore Sarawak," in *Atlas of Seismic Stratigraphy*, Bally, A.W. (Ed.), AAPG Studies in Geology 27, pp.168-173.

F. Jerry, L. (1993). Development Geology Reference Manual. In D. Morton-Thompson, & A. M.Woods, *AAPG Methods in Exploration Series, No.10* (p. 548). AAPG.

Hartmann, D. J., & Beaumont, E. A. (2000). Predicting reservoir system quality and performance. In E. A. Beaumont, & N. H. Foster, *Exploring for Oil and Gas Traps* (p. 1150). AAPG.

Ingham, F. T. & Bradford, E. F. 1960. The geology and mineral resources of the Kinta Valley, Perak. *Geological Survey Federated Malaya* 9.

Kadir, A., Pierson, J. B., Harith, Z. Z., & Chow, W. S. (2009). Kinta Valley Limestone: Clues for a New Play? *AAPG Convention* .

King, T. K., Chung, E., & AlJaaidi, O. (June 2010). Evolution and controlling factors of Miocene Carbonate build-up in Central Luconia, SE Asia: Insights from integration of geological and seismic characterization.

Lucia, F. J. (1996). Rock-Fabric / Petrophysical Classification of Carbonate Pore Space for Reservoir Characterization. *AAPG Buletin* , pp.1275-1300.

Raj, J.K., Tan, D. N. K. & Wan Hasiah Abdullah 2009. Cenozoic Stratigraphy. In Hutchison, C. S. & Tan, D. N. K. (eds.) *Geology of Peninsular Malaysia*. Universiti Malaya and Geological Society of Malaysia Publication, Kuala Lumpur, pp.133-173.

Schlumberger. (n.d.). Retrieved February 17, 2014, from Technical Challenge: http://www.slb.com/services/technical_challenges/carbonates.aspx

Wee, P. Y., & Liew, S. L. (1988). Development Planning of the F6 Gas Field in Central Luconia, Offshore Sarawak, Malaysia. *Society of Petroleum Engineer* .

APPENDINCES

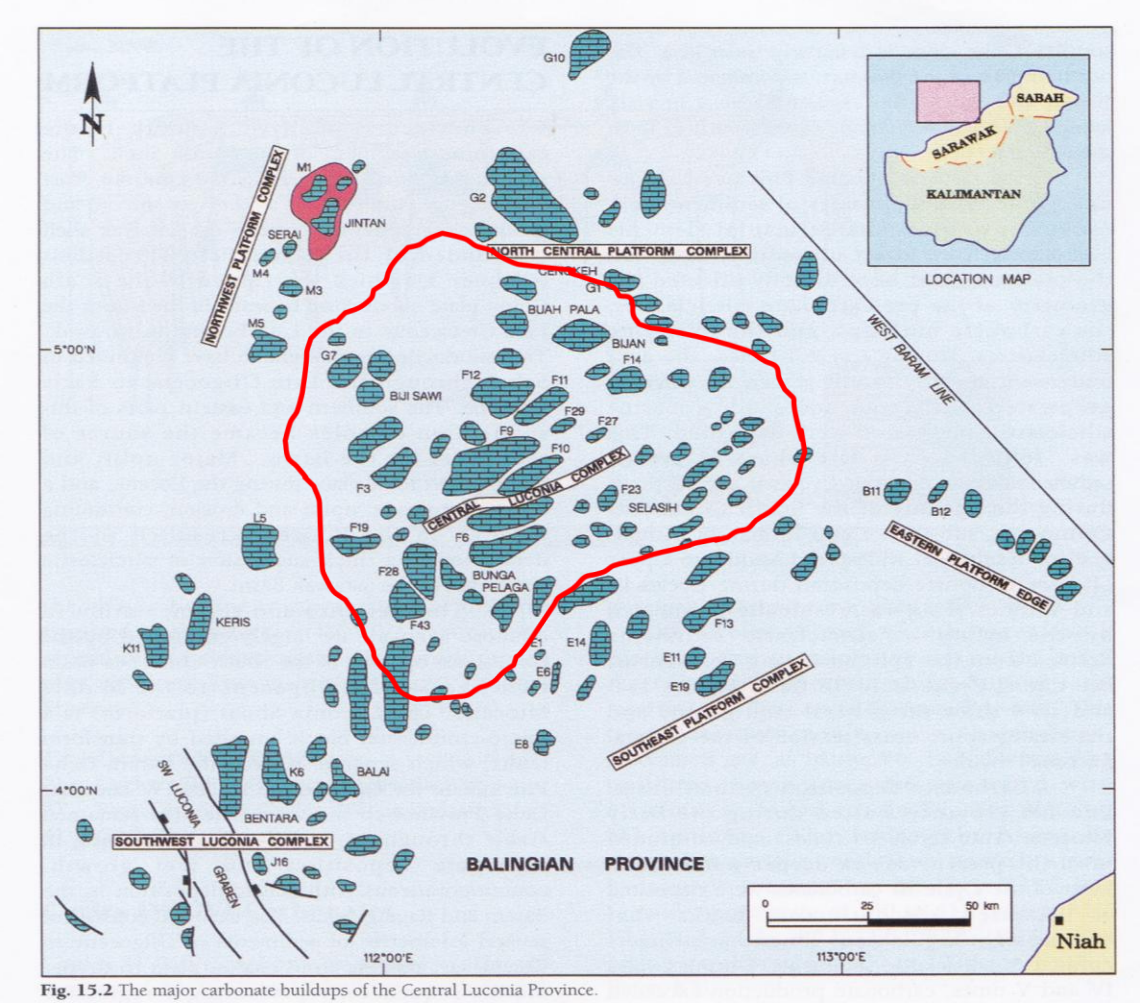

Fig. 15.2 The major carbonate buildups of the Central Luconia Province.

Figure 7.1 : Aerial Map of Central Luconia Province, showing the offshore carbonate buildups. F-fields is situated within the red circle.

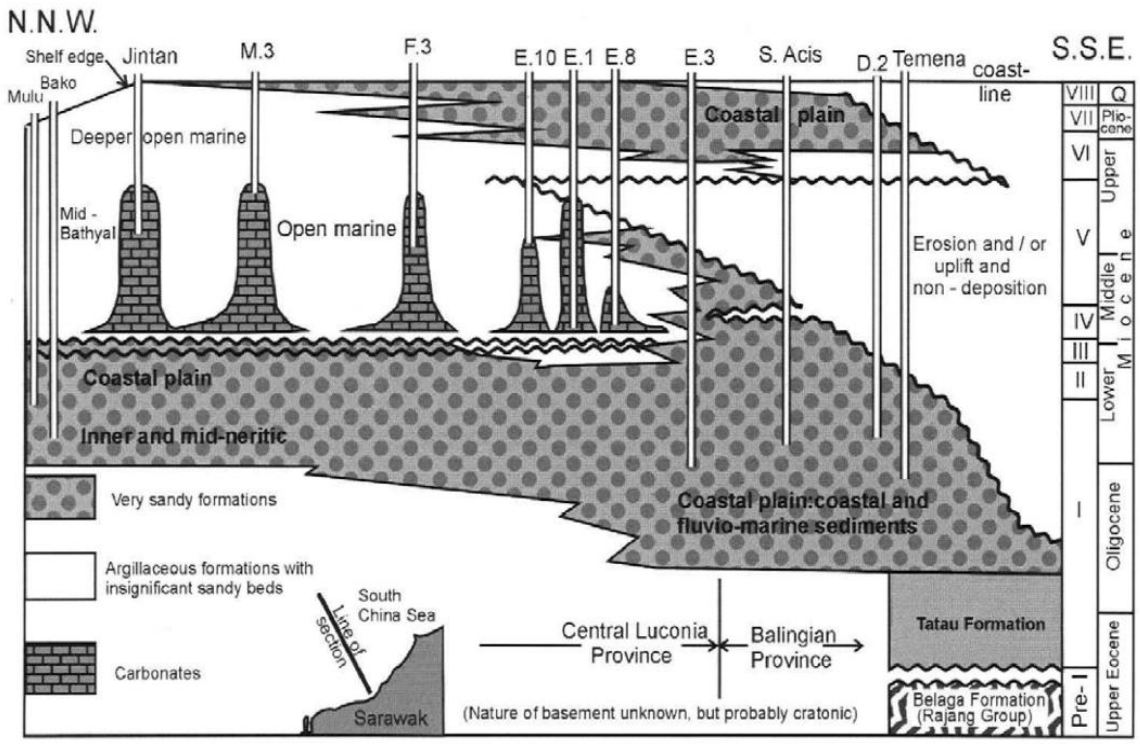

Figure 7.2 : Seismic section cutting across the M, F and E field of Central Luconia Basin.

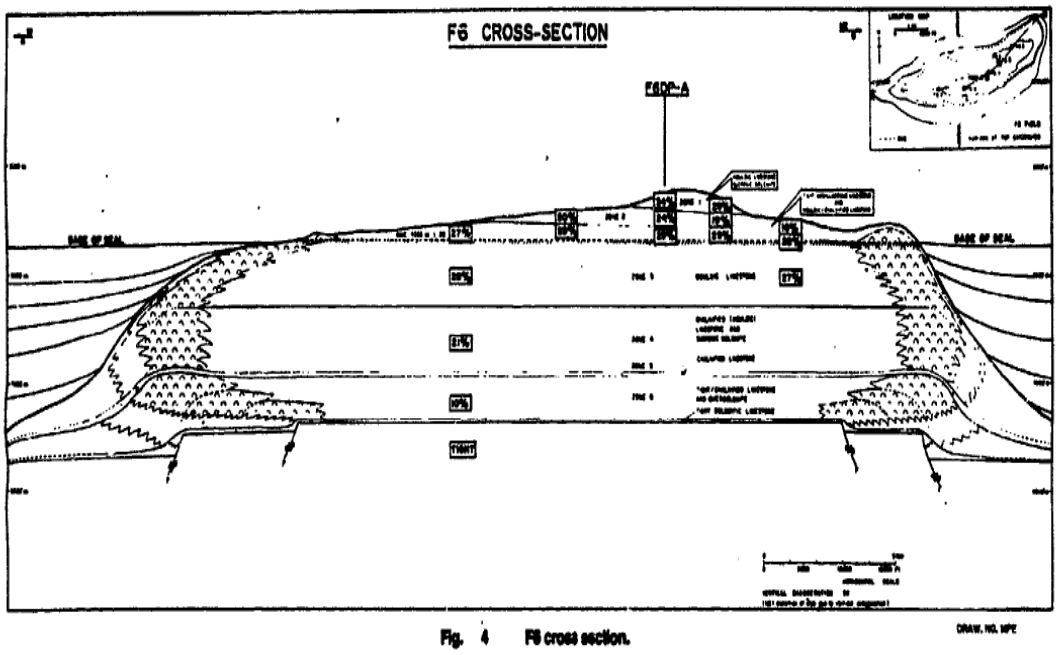

Figure 7.3 : Cross section of F6 field dividing into 3 major zones.